Received: 5 June 2020 | Revised: 7 September 2020 | Accepted: 30 September 2020

DOI: 10.1111/jace.17544

Journal of the American Ceramic Society

INVITED FEATURE ARTICLE

Processing of MAX phases: From synthesis to applications

Jesus Gonzalez-Julian

Forschungszentrum Jülich GmbH, Institute of Energy and Climate Research, Materials Synthesis and Processing (IEK-1), Jülich, Germany

Correspondence
Jesus Gonzalez-Julian, Forschungszentrum Jülich GmbH, Institute of Energy and Climate Research, Materials Synthesis and Processing (IEK-1), 52425 Jülich, Germany.
Email: j.gonzalez@fz-juelich.de

Funding information
Bundesministerium für Bildung und Forschung, Grant/Award Number: MAXCOM 03SF0534

Abstract

MAX phases are a large family of materials with more than 150 different compositions that have been extensively investigated during the last 25 years. They present a layered structure and a unique combination of properties, bridging the gap between metallic and ceramic properties. However, despite their excellent response of some compositions at high temperature—excellent oxidation resistance up to 1400°C under corrosive environment, good damage and radiation tolerance, thermal shock resistance, and self-crack healing—their transfer to applications has been limited by three main factors: i) complexity of this large family of materials, ii) unavailability of highly pure commercial powders, and iii) extensive time to license products in strategic fields such as nuclear or aviation. In this article, the main properties and synthesis routes are reviewed, including solid state reaction methods, physical vapor deposition (PVD) techniques and molten salt processes. Emphasis is given to processing routes for developing different structures such as dense bulk samples, ceramic matrix composites, foams with different porosity, coatings by PVD and thermal spray technologies, and near net shaping by slip casting, injection molding, and additive manufacturing. Well-known and novel potential applications are described such as structural materials for high temperature applications, protective coatings and bond-coats for gas turbines, accident tolerant fuel cladding in nuclear power plants, solar receiver in concentrated solar power systems, electrical contacts, catalyst, and joining material. Finally, high impact investigations and future challenges are listed in order to facilitate the transfer of MAX phases to the market.

KEYWORDS

applications, MAX phases, processing, synthesis

1 | INTRODUCTION

MAX phases are well-known and established due to their unique combination of properties and versatility, but this family of materials has experienced several ups and downs during its short history, including even being referred to with different names. Extensive work was carried out in the early 1960s in Vienna (Austria) by Wolfgang Jeitschko and Hans Nowotny, who discovered in more than 100 new carbides and nitrides.[1] Among them, they reported a new class of ternary systems, based on a transition metal (M), a metalloid (Me), and carbon (C), with a similar crystal structure to carbon-stabilized β-manganese phase, that is, Mo_3Al_2C. They were classified as "H-Phases" due to their hexagonal crystal structure, and some compositions

were in the systems of Ti-Al-C, V-Al-C, Nb-Al-C, Cr-Al-C, Ti-Sn-C, and V-Ga-C. They also synthesized Ti_2AlN through the reaction of TiN, Ti, and Al powders using hot-pressing, as well as other H-Phases in the Ti-Ge-N and Ti-Sn-N systems.[2] More phases were discovered during the following years. For example, Ti_3SiC_2 was hot pressed at 1200°C in helium atmosphere, although other phases such as $TiSi_2$, SiC, TiC_{1-x}, and $Ti_5Si_3C_{1-x}$ were also formed.[3] In spite of this significant discovery, H-Phases went practically unnoticed during the following decades.[4] However, the story of these phases changed in 1996, when Michel W. Barsoum et al published "Synthesis and characterization of a remarkable ceramic: Ti_3SiC_2".[5] In this work, fully dense predominantly single phase Ti_3SiC_2 was obtained by reactive hot-pressing of TiH_2, SiC and graphite powders at 40 MPa and 1600°C for 4h. Microstructural characterization, oxidation resistance, mechanical properties, machinability, and thermal and electrical properties showed that the material had a unique combination of ceramic and metallic properties. The main breakthrough of this work was drawing attention to this family of materials, exploding the interest on these phases. During the following years, more compositions were predicted and synthesized, exhibiting the same crystal structure with "$M_{n+1}AX_n$" as general formula, where "M" corresponds to a transition metal, "A" is an A-group element, "X" is C and/or N, and "n" is equal to 1, 2, or 3 (Figure 1).[6] This was the first time that the term "$M_{n+1}AX_n$" was used, which was lately simplified to "MAX", leading to the now known MAX phases. All MAX phases present a hexagonal crystal structure (space group P63/mmc), where layers of edge-shared M_6X-octahedra are interleaved with layers of "A" elements, which are located at the center of trigonal prisms (Figure 1). The "n" value indicates the number of "M" layers separating the A layers. The M-X bonds are exceptionally strong due to a mixed metallic-covalent nature, meanwhile the M-A bonds are relatively weak. This unique crystal structure is responsible for the characteristic layered structure (Figure 2) and the unique combination of properties, bridging the gap between ceramics and metals.[7]

More than 150 different compositions have been discovered so far and the number increases regularly thanks to the combination of experimental works and theoretical calculations (eg, by density functional theory (DFT)).[8] Nevertheless, not all possible combinations are thermodynamically stable. For example in the Ti-Al-C system, Ti_2AlC and Ti_3AlC_2 (n = 1 and 2, respectively) are stable in a wide range of temperatures, but in systems such as Cr-Al-C and Ti-Si-C only one "n" value is stable, that is, Cr_2AlC and Ti_3SiC_2. Additionally, a practically unlimited number of solid solutions are possible by substitutions on "M", "A", and/or "X" sites.[9,10,11,12,13] Based on the huge number of potential permutations, compositions of thermodynamically stable solid solutions have not been defined and maximum solubilities for each system are not known. Some elements present low solubility, that is, < 5 at.% of Cr in Ti_2AlC,[14] meanwhile others cover the whole range, that is, $Ti_3(Al_{1-x}Si_x)C_2$ for $0 < x < 1$.[11] Interestingly, some solid solutions can be synthesized even though the end-member MAX phases are unstable. For example, $(Cr_{2/3}Ti_{1/3})_3AlC_2$ and $(Cr_{5/8}Ti_{3/8})_4AlC_3$ have been reported,[15,16] whereas Cr_3AlC_2, Cr_4AlC_3, and Ti_4AlC_3 are not thermodynamically stable. The stability of the solutions is attributed to the formation and higher stability of ordering of two M elements onto the two different M Wyckoff sites of the crystal structure.[16] M ordering has been demonstrated for other compositions such as $(Cr_{0.5}V_{0.5})_3AlC_2$, $(Mo_{2/3}Ti_{1/3})_3AlC_2$, $Ti_{0.5}V_{0.5}AlC_2$, $(Nb_{0.5}V_{0.5})_2AlC$, or $(Ti_{1-x},Zr_x)_2AlC$.[17,18,14,19]

Since the year 2000, research on MAX phases has been dominated by the synthesis of new phases and solid solutions, calculation and subsequent deeper understanding of the structures, bonding and defects, as well as the characterization of properties. Much of this knowledge is carefully collected

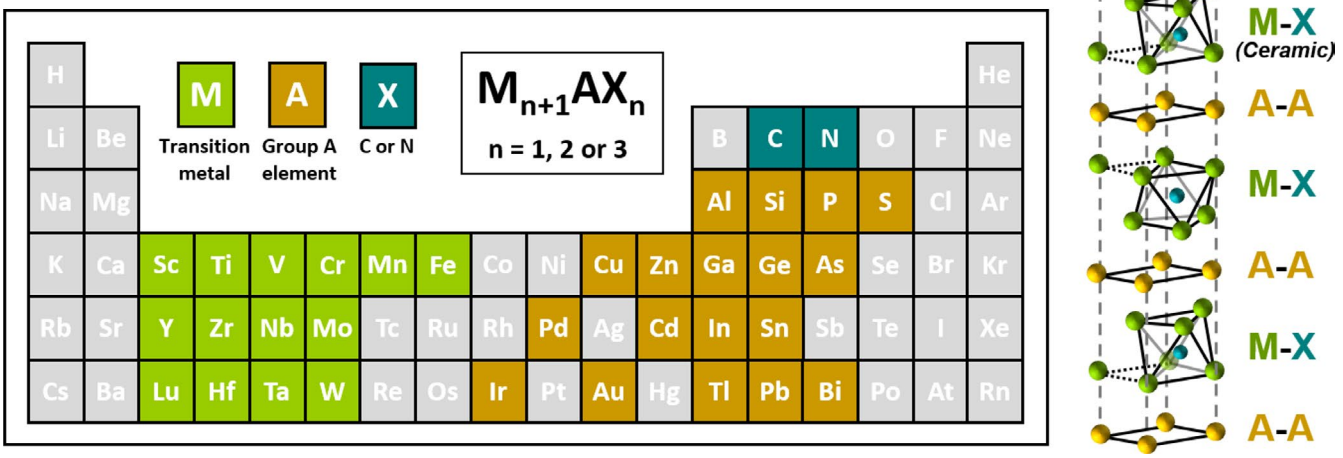

FIGURE 1 Elements of the Periodic Table found in MAX phases and unit cell for n = 1 [Color figure can be viewed at wileyonlinelibrary.com]

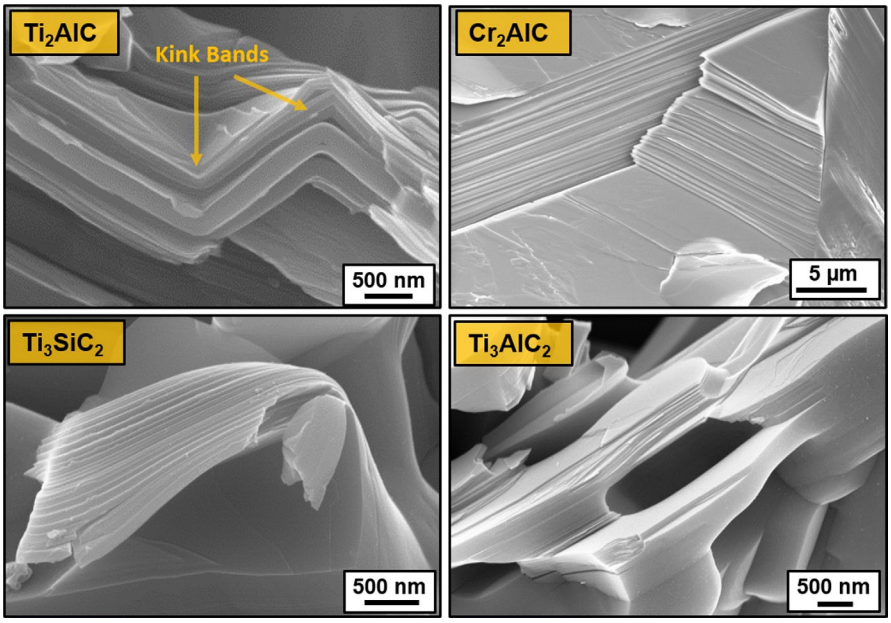

FIGURE 2 SEM pictures of the characteristic layered structure and mechanical response of Ti_2AlC, Cr_2AlC, Ti_3SiC_2, and Ti_3AlC_2 [Color figure can be viewed at wileyonlinelibrary.com]

in an outstanding book published in 2013 by Barsoum with the title "MAX phases: Properties of Ternary Carbides and Nitrides",[20] a must for all the researchers who want to be introduced to the MAX phases.

While 20 years is a realistic time to find some applications in the market,[21] but unfortunately their transfer to widespread industrial applications has not happened yet. One notable exception is Cr_2AlC, which is used in pantographs for high-speed trains in China. Interestingly, Kanthal® (Part of Sandvik Group®) commercialized MAX phase powders a few years ago, mostly Ti_2AlC and Ti_3SiC_2, under the MAXTHAL® license. However, the production of MAXTHAL® powders is currently inactive. Numerous applications have been proposed and tested, such as replacement for graphite at high temperature, heating elements, high temperature foil bearings, gas burner nozzles, tooling for dry drilling of concrete, ignition devices, and electrical contacts,[20] but as mentioned, they are not commercialized yet. This lack of final products might be attributed to three main reasons: i) complexity of this large family of materials, ii) extensive time to license products in strategic fields such as nuclear or aviation, and iii) unavailability of highly pure commercial powders. However, transferring MAX phases to the market is expected soon, and this period might be triggered by the discovery in 2011 of a new family of 2-Dimensional materials—referenced as MXenes -,[22] for which MAX phases are currently the only precursor.

2 | MIND THE GAP

The main characteristic of MAX phases is their unique combination of properties, filling the gap between ceramics and metals. Mechanical behavior,[23,24] oxidation resistance,[25] and tribological and magnetic properties[26,27] have been reviewed, but in this section the main features of the most attractive compositions (Ti_3SiC_2, Ti_2AlC, Ti_3AlC_2, and Cr_2AlC) are briefly described to facilitate the understanding and their potential applications. Unfortunately, the combination of properties is sometimes misunderstood, that is, high hardness as ceramics, elevated and congruent melting point, and/or high thermal conductivity as metals.

2.1 | Lightweight

The density of MAX phases varies typically between 4 and 6 g/cm^3, although some compositions such as Ta_2GaC and Hf_2TlC present larger values, 13.05 g/cm^3 and 13.65 g/cm^3, respectively. Nevertheless, Ti_3SiC_2, Ti_2AlC, Ti_3AlC_2, and Cr_2AlC present relatively low densities, 4.52 g/cm^3, 4.11 g/cm^3, 4.51 g/cm^3, and 5.23 g/cm^3, respectively. These density values are comparable to most of the advanced structural ceramics such as Al_2O_3 (4.0 g/cm^3), SiC (3.2 g/cm^3), Si_3N_4 (3.2 g/cm^3), ZrB_2 (6.0 g/cm^3) or 8YSZ (6.1 g/cm^3), and lower than high-temperature superalloys as EMP102 (9.2 g/cm^3), Inconel 738 (8.1 g/cm^3), RENE N5 (8.6 g/cm^3), or RENE N6 (9.0 g/cm^3). This factor is determinant in fields such as transportation, in particular for airplanes and space vehicles.

2.2 | Mechanical properties

The mechanical response of MAX phases has been largely explored, and is probably the most intriguing property. Typically, layered solids lack the five independent slip systems needed for ductility.[24] However, in MAX phases, basal plane dislocations (BPD) are abundant, mobile and

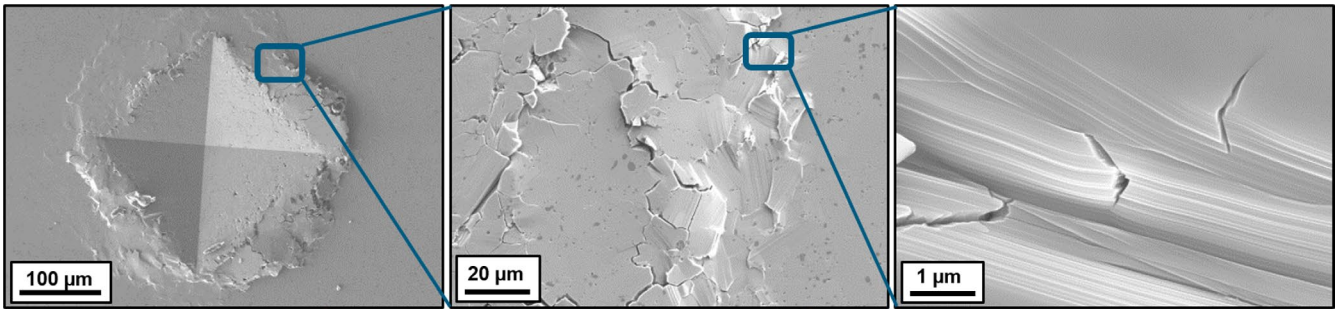

FIGURE 3 SEM micrographs at different magnifications of a Vickers indentation on Cr_2AlC polished surface [Color figure can be viewed at wileyonlinelibrary.com]

able to multiply at room temperature. Confining the dislocations to the basal planes provokes kink band (KB) formation, a characteristic of MAX phases (Figure 2). These mechanisms have been accepted to describe the mechanical response, but a new mechanism referenced as ripplocations has been recently proposed and generated substantial debate in the community.[28] In contrast to dislocations, ripplocations have no Burgers vector and no polarity, but are based on the buckling of surfaces in Van der Waals layers.[29,30,31] MAX phases present high Young´s modulus with values around 300 GPa, but are relatively soft with hardness between 3 and 7 GPa. Interestingly, MAX phases exhibit a nonlinear, hysteretic, elastic behavior, which is unusual for stiff compounds. For example, polycrystalline Ti_3SiC_2 loaded cyclically in compression up to 1 GPa at room temperature, fully recover on the removal of the load, while dissipating about 25% (0.7 MJm^{-3}) of the mechanical energy.[32] Fracture toughness (K_{IC}) is one of the properties that has attracted the most interest due to quite respectable values.[20,24] Typically, K_{IC} of polycrystalline MAX phases ranges from 5 to 8 $MPa{\cdot}m^{1/2}$, although higher values have been reported for some compositions, such as Ti_3SiC_2 and Nb_4AlC_3.[33] The largest value reported so far is for textured Nb_4AlC_3, achieving K_{IC} of 17.9 and 11.5 $MPa{\cdot}m^{1/2}$ when the load was applied perpendicular or parallel to the basal planes.[34]

The mechanical response at elevated temperature is particularly interesting due to brittle to plastic transition (BPT) around 1000°C-1100°C, depending on the composition and microstructure. Below the BPT they are brittle as ceramics, but above it MAX phases are plastic, with strain failures up to 25% at low strain rates.[24,35,36] Failure is mainly caused by damage accumulation in the form of cavitations, pores, microcracks, and delamination.[37,38,39] Creep resistance has been reported for Ti_3SiC_2,[37,40] Ti_2AlC,[38] Ti_3AlC_2,[41] and recently for Cr_2AlC,[42] and Ti_2AlN.[43] Primary, secondary, and tertiary creep take place in the temperature range between 1000 and 1300°C, with activation energies in the range of 400 to 550 kJ/mol, and stress exponents (n) of ~2, indicating a creep mechanism controlled by grain boundary sliding. TEM observations suggest the formation of numerous stacking faults, dislocations that are mainly confined in the basal planes, and original lenticular non-planar defects.[41] Furthermore, MAX phases are not susceptible to thermal shock, where residual strength of as-quenched samples decreases gradually without any catastrophic failure. This effect has been observed for Cr_2AlC,[44,45] Ti_3SiC_2,[5,46,47] Ti_3AlC_2,[46,48] Ti_4AlN_3,[49] V_2AlC,[50] and Ti_3GeC_2.[51] Interestingly, an "abnormal" thermal shock behavior has been detected for most of these composition at temperatures higher than 900°C, where strength of the quenched samples increases with temperature. The mechanisms are still under debate but correlated to the self-healing effect of MAX phases and the compressive stresses on the specimen surface caused by the formation of an oxide layer.[48]

2.3 | Damage tolerance

MAX phases exhibit better damage tolerance than other advanced ceramics. This effect can be observed by performing Vickers indentation. Instead of crack formation and propagation, other mechanisms such as delamination, kinking of individual grains, and grain pullouts are activated in the nearby area of the indent (Figure 3). In addition, Weibull modulus of MAX phases is high, that is, 29 for polycrystalline Ti_3SiC_2,[52] although more experiments are required.

2.4 | Melting point

MAX phases melt incongruently, forming typically M-X specimens (carbides or nitrides) and A-rich liquids or intermetallics at high temperature. The temperature of this incongruent melting strongly depends on factors such as purity and environment. For example, Ti_3SiC_2 is quite refractory in vacuum, with a decomposition above 2300°C,[7,20] but that drops up to ~1000°C under oxidizing environments. The $M_{n+1}X_n$ layers are stable, whereas the A layers are weakly bonded and mobile, so the "A" element typically diffuses out of the structure at elevated temperature. Nevertheless, this drawback at

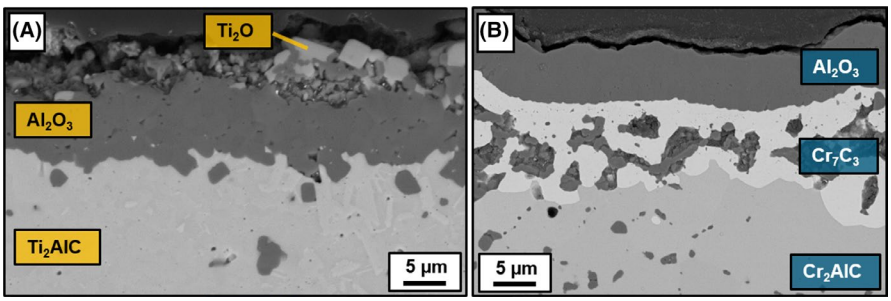

FIGURE 4 Representative SEM micrographs of polished cross sections after oxidation at 1200°C of (A) Ti_2AlC and (B) Cr_2AlC [Color figure can be viewed at wileyonlinelibrary.com]

first glance causes one of the most interesting responses of MAX phases at elevated temperature when the "A" element is Al and Al_2O_3 is formed under oxidizing environments.

2.5 | Oxidation resistance

In general, MAX phases oxidize at relatively low temperature (~600°C) according to the following reaction:

$$M_{n+1}AX_n + bO_2 \rightarrow M_{n+1}O_x + AO_y + X_nO_{2b-x-y} \quad (1)$$

Consequently, most of them are not suitable for high temperature applications under oxidizing atmospheres. However, some compositions that contain Al as the "A" element are able to form an external and adherent α-Al_2O_3 layer, which protects against further inward oxygen diffusion at temperatures up to 1400°C.[53] Unfortunately, not all Al-based MAX phases form an external protective alumina layer due to the "competition" between the oxidation of the "M" and "A" elements.[25] Ti_2AlC, Ti_3AlC_2 and Cr_2AlC form protective Al_2O_3 scales, but V_2AlC,[54,55] Ta_2AlC[56] and Nb_2AlC[57] form M-oxides such as V_2O_5, Ta_2O_5 and Nb_2O_5, respectively, at low temperatures (600°C-900°C). Consequently, only Ti_2AlC, Ti_3AlC_2 and Cr_2AlC are considered to operate under aggressive environments at high temperatures (900°C-1400°C) for extended periods. After some years of discussions,[20] the alumina scale growth was shown to be controlled by grain boundary diffusion, leading to cubic oxidation kinetics instead of parabolic.[58] Nevertheless, recent investigations claim that only the formation of a continuous Al_2O_3 layer leads to cubic oxidation kinetics, meanwhile a discontinuous alumina scale entails parabolic kinetics since oxygen can continuously diffuse inwards.[59] Additionally, the oxidation response is strongly influenced by factors such as particle size, orientation, secondary phases (carbides and intermetallics as well as Si, Fe, or S elements in ppm), Al/M ratio, and surface roughness.[25,20,60,61,62,63]

Ti_2AlC is the most studied composition and has attracted high attention from industry. In fact, a Ti_2AlC heating element was already reported by Sundberg et al in 2004 due to excellent response after 8000 thermal cycles at 1350°C in air.[64] In this case, a 15 μm protective alumina layer was formed on the surface during use. The adhesion of the alumina scale is of significant importance for high temperature applications. High temperature alloys typically present high coefficients of thermal expansion (CTE),> 13×10^{-6} K^{-1}, whereas α-Al_2O_3 has a lower value, 8-10 $\times 10^{-6}$ K^{-1}. The CTE mismatch generates thermal stresses at the interface, leading to spallation of the oxide scale. These thermal stresses are notably reduced for Ti_2AlC since its CTE is 8.2×10^{-6} K^{-1}. However, the main drawback of Ti_2AlC—as with Ti_3AlC_2—is the oxidation of the "M" element at temperatures as low as 600°C, forming rutile (TiO_2). As temperature increases the oxidation of the "A" element is favored, leading to the formation of an alumina scale that controls the oxidation kinetics. As a result, at temperatures between 1000°C-1300°C, the outer scale surface is composed of an alumina layer containing some TiO_2-rich nodules that generally do not seem to increase (Figure 4A). This configuration is quite stable up to temperatures around 1350°C for long times (>10^3 hours), but at higher temperatures formation of Al_2TiO_5 and presence of cracks limit the exposure time.[65] Cr_2AlC exhibits also a good oxidation response at temperatures between 1000°C and 1300°C, following cubic kinetics. The main advantage of Cr_2AlC in comparison to Ti_2AlC is the limited oxidation of the "M" element. Consequently, a dense, continuous, adherent,[66] and protective alumina layer is formed at temperatures up to 1300°C under oxidizing atmospheres. On the other hand, the main drawback is the formation of a porous Cr_7C_3 layer between the alumina scale and the Cr_2AlC at temperatures higher than 1150°C (Figure 4B). This porous layer is critical although it survives hundreds of hours at 1300°C in air,[67] but a realistic operating temperature for Cr_2AlC under long exposure times should not exceed 1200°C. In addition, Cr_2AlC has a CTE of 12.0 - 13.3 · 10^{-6} K^{-1}—the largest of the MAX phases—which generates more thermal stresses with the alumina layer, but opens the possibility to protect some refractory alloys against type I and II low temperature hot salt corrosion.[68,69]

Presence of water vapor at high temperature does not seem to greatly influence the scale formation and growth kinetics.[62,70] The oxidation resistance of Ti_2AlC and Cr_2AlC under more realistic environmental conditions using a burner rig has been reported.[71,72] Ti_2AlC was tested using a high pressure burner rig at 6 atm, 25 m/s, approx. 10% water

vapor at 1100, 1200, and 1300°C. The cubic rate constants were approx. 20% of those measured under static conditions, which was cause by a small recession of the initial TiO_2 and $TiAl_2O_5$ on the alumina layer and their subsequent volatilization as $TiO(OH)_2$.[71] Recently, dense Ti_2AlC was coated with porous YSZ as thermal barrier coating material, and tested in a jet fuel burner at high velocity of 100 m/s using 5h cycles.[73] No coating spallation or surface recession was detected after 500 hours, where the 20 μm alumina scale remained intact under the YSZ face, about twice in thickness that producing failure for TBC/superalloy systems. Regarding Cr_2AlC, samples were tested under severe thermal gradient conditions at 1200°C using a gas burner rig with gas velocity around 4-5 m/s. Cr_2AlC survived under these conditions thanks to the formation of a 5 μm-thick continuous, stable, and adherent alumina layer.[72] The mechanical adhesion of the different interfaces formed, Cr_2AlC/Cr_7C_3, and Cr_7C_3/Al_2O_3, was characterized by micro-cantilever fracture tests, revealing that the excellent interlocking is caused by the combination of low internal strain due to similar CTEs and the convoluted interface.[66]

2.6 | Crack self-healing

The protective alumina layer, which is formed at temperatures between 900 and 1300°C under oxidizing environments, entails a volume expansion. Besides, alumina has similar CTE and Young´s modulus values compared to most MAX phases, thus they are suitable for crack self-healing. It was reported for the first time in 2008, when a crack with an approx. 7 mm length and an average width of 5 μm in Ti_3AlC_2 was healed at 1100°C for 2 hours. [74] Other MAX phases, such as Ti_2AlC and Cr_2AlC,[63,75,76,77,78] have exhibited this response under similar conditions, but this effect was not observed for other phases such as Ta_2AlC.[79] Ann-Sophie Farle et al reported the different criteria for self-healing MAX phases as well as potential candidates, including the adhesion and cohesion energies, CTE and stresses, and Young´s modulus.[80] The healed cracks have sufficient mechanical integrity to make subsequent cracks from elsewhere upon reloading after the healing process.[81] This effect has determinant consequences on the mechanical properties of MAX phases, such as after the impact of foreign objects [82] or exhibiting abnormal thermal shock behavior.[44,46]

2.7 | Corrosion resistance

MAX phases have been evaluated under different corrosive environments and the response was good. Ti_3AlC_2 and Ti_2AlC were tested against molten Na_2SO_4 salt for 20 h hours at 900 and 1000°C resulting in weight gains of 0.15 and 0.45 $kg{\cdot}m^{-2}$, respectively, meanwhile Cr_2AlC exhibited a weight gain of only 8 0.10^{-4} and $1.5 \cdot 10^{-3}$ $kg{\cdot}m^{-2}$ under the same conditions. [83,84,85] Similar superior corrosion resistance was also reported for Cr_2AlC by K. Van Loo et al in a different corrosive medium.[86] In that work, Ti_2AlC, Ti_3SiC_2, Cr_2AlC, Nb_4AlC_3, $(Nb,Zr)_4AlC_3$, different SiC grades and a 40 vol% Fe/60 vol% $(Nb,Zr)_4AlC_3$ cermet were exposed to a KNO_3-$NaNO_3$ molten solar salt for 1000 hours at 600°C. Under these conditions, no alumina scale was formed leading to considerable corrosion of the materials except in the case of Cr_2AlC, which was protected by a micrometer-thin layer of Cr_7C_3. Furthermore, different MAX phases were screened with respect to their interaction with oxygen-poor ($C_O \sim 5 \times 10^{-9}$ mass%), static and fast-flowing (v ~ 8 m/s) liquid lead-bismuth eutectic (LBE) for at least 1000 hours at 500°C.[87,88] No evidence of LBE dissolution attack was observed, despite the absence of a continuous external oxide scale. The local LBE interaction observed with the Zr-rich MAX phases consisted in the partial substitution of Al by Pb/Bi in the crystal structure and the in situ formation of $(Zr,Ti)_{n+1}(Al,Pb,Bi)C_n$ solid solutions. Moreover the interaction of Zr-based MAX phases with static liquid LBE was accompanied by the dissolution of parasitic intermetallic phases, facilitating further LBE ingress into the bulk material. Interestingly, the selected MAX phases presented a better resistance to both dissolution corrosion and erosion in comparison to 316L stainless steels.[87] Surprisingly, only one work, involving Ti_2AlC, has recently been published about corrosion by calcium-magnesium-aluminum-silicate (CMAS) sand, despite the high potential of MAX phases for gas turbine applications.[89] Ti_2AlC pellets were exposed to molten CMAS at 1250°C for different hours and the melt was significantly suppressed by the alumina scale.

2.8 | Coefficient of thermal expansion

MAX phases present a hexagonal crystal structure, with a consequent CTE anisotropy between *a* and *c* planes. Typically, the average CTE ranges between 8×10^{-6} K^{-1} and 10×10^{-6} K^{-1}, although some compositions have lower or higher values.[20] For example, Nb_4AlC_3 presents an average CTE of 6.7 - 7.2 $\times 10^{-6}$ K^{-1},[90,91] meanwhile Cr_2AlC varies between 12.0 and 13.3 $\times 10^{-6}$ K^{-1}.[92,93] Solid solutions modifies the CTE, as reported for $Cr_2(Al_x,Ge_{1-x})C$ in the 25°C-800°C temperature range.[92] The thermal expansion of the *a* axis remains constant at 14×10^{-6} K^{-1}, whereas the *c* axis decreases constantly from 17×10^{-6} K^{-1} for Cr_2GeC to approx. 12×10^{-6} K^{-1} for Cr_2AlC. The $Cr_2(Al_{0.75},Ge_{0.25})C$ composition has an equal CTE in both axes, minimizing the thermal residual stresses. In general, the CTE of MAX phases lies between non-oxide ceramics and metals (Figure 5), and tend to be a good match for conventional Thermal Barrier

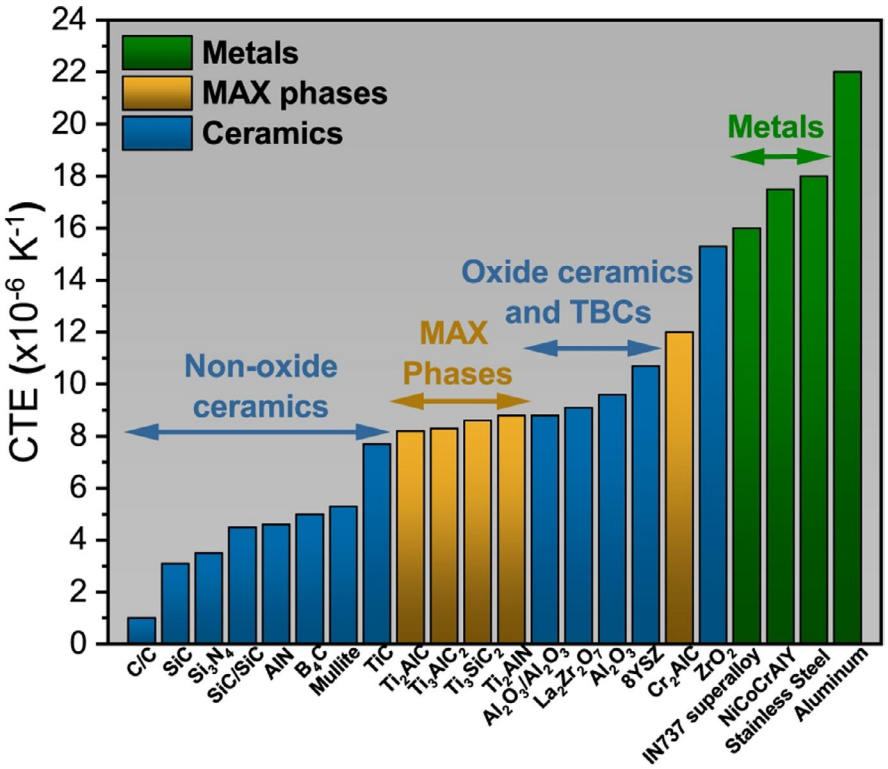

FIGURE 5 Coefficient of Thermal Expansion (CTE) of representative ceramics, MAX phases and metals [Color figure can be viewed at wileyonlinelibrary.com]

Coatings (TBCs) such as YSZ (10-11 × 10^{-6} K^{-1}) and the thermally grown oxide (TGO, α-Al_2O_3; 8.5-9.5 × 10^{-6} K^{-1}). In fact, the good CTE match reduces around 1/7 the interfacial thermal stresses in comparison to conventional high temperature metallic systems. [94,95]

2.9 | Radiation tolerance

Ti_3SiC_2, Ti_2AlC, Ti_3AlC_2, Cr_2AlC, V_2AlC, Zr_2AlC, Zr_3AlC_2, and Nb_4AlC_3 have been proposed as accident tolerant fuel (ATF) claddings in third-generation light-water reactors (LWRs) and future fourth-generation fission plants due to the good radiation tolerance at room and high temperature. Ti_3SiC_2 was the first MAX phase to be investigated using heavy ions of different energies at room temperature to understand and differentiate between the nuclear and electronic interactions.[96] Elastic collisions lead to the amorphization of the Ti_3SiC_2, sputtering of the grain boundaries, and preferential sputtering as a function of the crystal orientation, whereas the electronic interactions induce the amorphization of only Ti_3SiC_2 and the expansion of the unit cell along the *c* axis. Expansion of the *c*-lattice parameter, as well as irradiation-induced hardness that could be annealed at 800°C, was also observed by Liu et al after irradiation to a maximum dose of 3.25 dpa (displacement per atom) of Al-doped Ti_3SiC_2 with high-energy Kr and Xe ions.[97,98] Ti_2AlC and Ti_3SiC_2 show good irradiation resistance up to 0.1 dpa, providing evidence for the MAX phases´ dynamic recovery at temperatures as low as 695°C.[99] Interestingly, elevated temperatures provide sufficient energy to allow migration and recombination of point defects, annealing the damage during irradiation.[100] Ti_3AlC_2 also shows excellent tolerance to irradiation damage over a wide fluence range. No amorphization occurs upto 31 dpa, although the nanolamellar structure disappeared through the formation of antisite defects and a phase transformation from α- to β Ti_3AlC_2 phase.[101] Similar phase transitions from hcp to fcc structures were found in Ti_2AlN, Ti_2AlC, and Ti_4AlN_3, where the formation of intermediate γ-phases is driven by the production of cation antisite defects and a corresponding rearrangement of anions.[102] The occurrence of extended defects, including stacking faults, contributes to the transition from the intermediate γ-phases to fcc phases. Cr_2AlC has been also irradiated under different ions and temperatures, detecting a structural transition for irradiations above 1 dpa, although the structure is stable up to 5.2 dpa without obvious lattice disorder.[103] The structural transition and irradiation effects saturation are ascribed to irradiation-induced antisite defects (Cr_{Al} and Al_{Cr}) and C interstitials, with a potential transition from the initial phase to γ-Cr_2AlC.[103,104] Furthermore, Zr- and Nb-based MAX phases have been recently considered due to the small neutron cross-section of Zr and the favorable refractory metal properties of Nb.[105] The post-irradiation examination revealed that Zr_3AlC_2 and $(Zr_{0.5},Ti_{0.5})AlC_2$ have a superior ability for defect-recovery above 400°C, meanwhile the Nb_4AlC_3 does not show any appreciable defect recovery below 600°C. In addition, DFT calculations have shown that 413-MAX phases in general may not perform well under low temperature irradiation

conditions due to the preference for M:A antisites and C Frenkel pairs at the M-2 layer.[105]

2.10 | Tribological properties

The layered structure suggests a good tribological response. The first work published in 1996 reported a lubricious feel,[5] and a few years later an ultra-low coefficient of friction (μ) was measured for Ti_3SiC_2 basal planes ($2\text{-}5 \times 10^{-3}$) using a lateral force microscope.[106] However, the results reported later in polycrystalline samples have less attractive values. An exhaustive review was published by Gupta et al,[26] who also performed several investigations.[107,108,109,110] In general at room temperature, the wear rate (WR) was relatively high and almost linearly dependent to sliding distance, meanwhile the initial μ was low (< 0.2) but increased rapidly to larger values (>0.4). Certainly, the tribological response depends on several factors of the microstructure (grain size, purity, porosity, etc), the counter-body (metal, ceramic, hardness, etc), and the testing conditions (temperature, atmosphere, velocities, pressure, lubrication, etc).[26,111,112,113] Additionally, tribological response of polycrystalline MAX phases is controlled by complex tribochemical reactions.[26] At high temperatures, the tribological response is better, where initial μ is high (>0.6) but decreases with time to steady-state values (0.4-0.6) and WRs are typically low ($<10^{-5}$ mm^3/Nm).[108,109]

Tribological performance has been improved by adding secondary phases such as Al_2O_3, BN, B_4C, SiC, chopped SiC fibers, Ti_5Si_3, and Ag.[114,115,116,117,118] Ceramic particles improve the wear resistance due to their higher hardness and decentralization of shear stresses under the counter-body, meanwhile the addition of metallic particles modifies the tribochemistry reactions. Additionally, MAX phases have been recently added as reinforcing particles in metals [119,120] and polymers.[121,122] The composites present lower μ and WRs due to the mitigation of the abrasive wear and modification of the tribochemistry reactions.

2.11 | Electrical properties

MAX phases are metallic electrical conductors in which the resistivity increases linearly with temperature.[20] In most of the cases, the electrical resistivity at room temperature varies between 0.02 and 2.00 μΩ m.[23,49] Interestingly, some MAX phases present lower electrical resistivities than their metallic counterpart, that is, Ti_2AlC and Ti_3AlC_2 (0.20-0.35 μΩ m) and Ti (~ 0.4 μΩ m). Electrical conductivity is affected by particle size and by secondary phases/impurities, and solid solutions which lead to scattering. Regarding the Seebeck coefficient, MAX phases present small values—even negligible,[123] with no particular temperature dependence. Electrical resistivity, Hall Coefficients, Magnetoresistance, transport mechanisms, and Seebeck coefficients are explained in detail elsewhere.[20] Electrical conductivity of MAX phases is several order of magnitude higher than advanced ceramics, which has an important consequence for machinability and opens new solutions for electrochemical reactions and electrically heating-catalyst (EHC).[124,125]

2.12 | Thermal properties

MAX phases are considered good thermal conductors, with conductivities between 12 and 60 $W\ m^{-1}K^{-1}$.[23] The thermal response is extensively described elsewhere,[20] including the electron and phonon contributions as a function of temperature, rattler effect, role of defects, phonon density of states, heat capacities, and Debye temperatures. As with the electrical response, some MAX phases exhibit larger thermal conductivities than their corresponding transition metals.[20] The thermal response is the sum of the electron (K_e) and phonon (K_{ph}) conductivities, where each contribution depends on several factors such as temperature, composition (mostly the "A" element), grain size, secondary phases/impurities, and defect concentration.[20,126,127] Overall, MAX phases are good phonon conductors because of the M-X bonds, and particularly composition containing Al due to the lower scattering since it is light and mobile. Furthermore, phonon contribution is sensitive to the "n" value, where the distribution is wider as follows 211 > 312 > 413. Regarding the respond at high temperature (1300 K), Ti_2AlC presents one of the highest thermal conductivities thanks to its high K_{ph}. These experimental data are in good agreement with the calculation of K_{ph} using the Debye theory.[128]

2.13 | Machinability

MAX phases can be cut using a handsaw or a lathe due to the combination of low hardness, excellent damage tolerance, and good thermal shock resistance. Furthermore, they can be precisely machined by electrical discharge machining (EDM) thanks to their high electrical conductivity.[129] This is of special importance when compared to most of the advanced ceramic materials, where machinability is difficult, time consuming, and expensive due to their high hardness and brittleness. Melting and decomposition were found to be the material removal mechanisms during EDM machining of Ti_3SiC_2. As expected, material removal rate was enhanced by increasing discharge current and working voltage, but microcracks on the surface and loose grains in the subsurface were detected, degrading the strength and reliability.[130] The

cutting resistance and roughness of Ti_3SiC_2 are lower when compared with a middle-carbon steel, SM45C.[131]

3 | SYNTHESIS

The synthesis of MAX phases can be categorized in three main groups: i) Physical Vapor Deposition (PVD) techniques, ii) solid state reactions, and iii) molten processes. In general, the synthesis of MAX phases is relatively simple, but high yields (~> 95 wt%) are difficult because they coexist with other thermodynamically stable phases such as carbides or nitrides and intermetallics. Unfortunately, M-A-X phase diagrams are only available for some systems. The main limitation is the synthesis of large quantities of highly pure MAX phase powders, which has restricted their transfer to industry. PVD methods usually lead highly pure MAX phase coatings, but they are not suitable processes for powder production. Powders can be synthesized by liquid/solid-state reaction approaches, but more investigation is required to improve purity, scalability, reproducibility, and costs.

3.1 | Physical vapor deposition

Eklund et al published in 2010 an exhaustive review about thin-film processing of MAX phases, including PVD and other techniques, nucleation and growth mechanisms as well as resulting properties.[132] In general, three main methods have been considered to synthesize thin films with high purity and density: magnetron sputtering, cathodic arc deposition, and pulse laser deposition (PLD). Depositions have been mainly performed at substrate temperatures between 800 and 1000°C, which are high for some sensitive substrates such as certain steels.[132] Consequently, effort have been focused on the reduction of the deposition temperatures of some compositions such as Cr_2AlC (450°C),[133] V_2GeC (450°C),[134] or V_2AlC (600°C).[135] Magnetron sputtering is the most used PVD method thanks to the easy processing, high flexibility, good control over phase purity and composition. Individual targets, typically three for "M", "A", and "X" (graphite) elements, are commonly used and preferred for the individual and flexible control of elements.[136] On the other hand, a single target, either a MAX phase compound target or a composite target of "M", "A", and "X" elements in the desired MAX phase stoichiometry, is mostly considered for industrial processes due to simplicity and repeatability. In the case of MAX-nitrides, reactive sputtering using nitrogen gas as N source is typically used.[137] Synthesis can be performed in one step, which involves heating the substrate during the deposition and often leads to columnar growth. Another option is to deposit first a film with the desired MAX phase stoichiometry, and annealing treatment at high temperature to crystallize the MAX phase. In general, highly dense and pure thin films with thicknesses from few nanometers to several micrometers can be obtained by sputtering. Cathodic arc deposition has been less studied in comparison to sputtering techniques due to the higher complexity of the process and equipment. The process is based on the vaporization from typically three cathode targets (M, A, and X elements) caused by a pulsed high current and low voltage arc. The high energetic arc generates a high degree of ionization of the deposition flux, almost 100%, which might reduce the synthesis temperature.[138,139] This process leads to a fine control of the final composition and in some specific cases even lower synthesis temperature, such as for Ti_2AlN.[132] Thick films can be obtained due to the high degree of ionization, but the powerful energies produce a negative effect, which is the presence of macroparticles embedded into the film. The amount of macroparticles can be reduced using filters, but their presence is a common drawback of this technique. PLD has been less explored than other PVD techniques despite the high potential to deposit MAX phases at temperatures below even 300°C.[140] A high-power pulsed laser beam strikes a MAX phase single target in a high-vacuum chamber, vaporizing the MAX phase and depositing it on a substrate kept at a low temperature (25°C-800°C). PLD leads to high purities, but in the case of MAX phases, some carbides are typically detected between the nanometric MAX grains.[141] The ion-beam has several interesting effects on film thickness and composition, concentration gradients within the films and on conductivity and hardness.[141] However so far, no clear model can be presented, but the high potential of PLD appeals for further investigations.

3.2 | Liquid/solid state reaction

Liquid/Solid state reaction (SSR) is the most used method to synthesize MAX phases. This method is based on the reactions at high temperature between the elemental constituent starting powders or other precursors such as carbides (MX) or hydrides (MH). The synthesis temperature typically ranges between 1100°C and 1700°C and is carried out under protective atmosphere to avoid the oxidation. As "M" source elemental powders such as Ti for Ti_2AlC and Ti_3AlC_2, or Cr for Cr_2AlC are more commonly used, although carbides such as TiC and Cr_3C_2 are also good options. Another alternative is to use metal hydrides, such as TiH_2 or ZrH_2,[142] since they seem to be beneficial for compositions that are difficult to synthesize such as Zr_2AlC or Zr_3AlC_2.[143,144] However, the use of metallic hydrides might be dangerous because of the liberation of H_2 during the thermal process, so safety has to be strongly considered for large quantities. As "A" source, elemental powders such as Al or Si are extensively used due to the low prices, and an excess up to 20 at. % is added to

compensate their loss due to evaporation at high temperature. As "X" source, graphite is used for carbide-MAX phases due to its low price, although carbides can also be employed. In general, substoichiometric quantities of carbon, ranging between 1.0 and 0.9 at.%, reduces the formation of secondary phases, and, consequently, increasing the yield. In the case of nitride-MAX phases, nitrides are used as starting powders since nitrogen is a gas under standard conditions. In terms of processing, SSR is simple. Starting powders are homogenously mixed in ethanol, followed by drying and pressing of the powders. Afterwards, pellets are heated up under protective atmosphere for the synthesis. Several reactions take place during the thermal process,[145,146] so MAX phases typically coexist with carbides or nitrides and some intermetallic compounds. Among the different synthesis methods, pressureless synthesis (PLS), self-propagating high-temperature synthesis (SHS), hot-pressing (HP), hot isostatic pressing (HIP), spark plasma sintering (SPS), and microwave (MW) are briefly explained.

3.2.1 | Pressureless synthesis

PLS is one of the most common synthesis methods due to its simplicity.[145,147,148,149,150,151] The pellets are just placed in a crucible and heated under vacuum or argon atmosphere to temperatures around 1400°C for few hours. The formation of MAX phases starts around 1000°C, but the highest yield is achieved around 1300°C-1400°C. At higher temperatures some carbides or nitrides start to be detected due to the degradation of MAX phases. PLS leads to highly pure, around 95 wt%, and porous pellets with relative densities up to 90%–92%. This process is commonly used to produce powders, and is, therefore, often followed by a milling step. Figure 6 shows an example of a 500g batch of Cr_2AlC synthesized by PLS, followed by milling to obtain fine powders. In general, PLS is simple, cost-effective, flexible in terms of precursors, scalable to large quantities, and leads to relatively high purities. The limitations are related to the long thermal cycles, the inability to produce fully dense components, and the necessity of a milling step to obtain powders.

3.2.2 | Self-propagating High-temperature Synthesis

SHS is an attractive method that takes advantage of the highly exothermic reactions during the formation of MAX phases.[152,153,154,155] Basically, the precursors are homogeneously mixed and pressed to obtain green pellets with high densities. Then, an electric current passes through a tungsten filament to ignite the pellet under vacuum, to avoid the oxidation. Maximum external temperatures are around 1400°C with an average combustion wave velocity up to 10 mm/s.[154,156,157] The process is fast and self-sustainable, and leads to produce large quantities of powders, but the main drawback is the yield.[158,159] Several starting compositions have been tested for the Ti-Al-C system, but presence of carbides and other secondary phases is difficult to avoid due to the high combustion velocities and thermal gradients. Similar results have been reported for Ti_3SiC_2 and Cr_2AlC, where the formation of secondary phases is considerable.[152,160,161] SHS leads to porous pellets, although full densification can be achieved with a subsequent pressing step (around 500 MPa) when the sample is still hot. The main advantages of SHS are the simplicity, short times, scalability, low cost, and energy

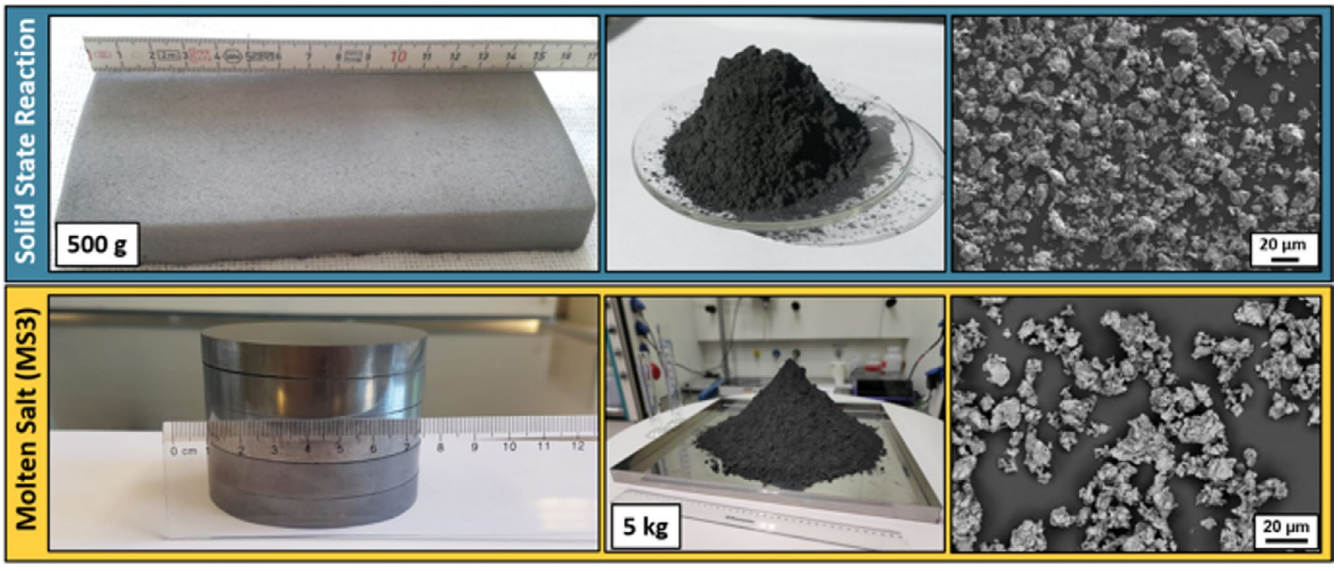

FIGURE 6 Photographs and SEM pictures of solid-state reaction for 500g of Cr_2AlC and Molten Salt Shielded Synthesis (MS3) for 5 kg of Ti2AlC to produce MAX phase powders [Color figure can be viewed at wileyonlinelibrary.com]

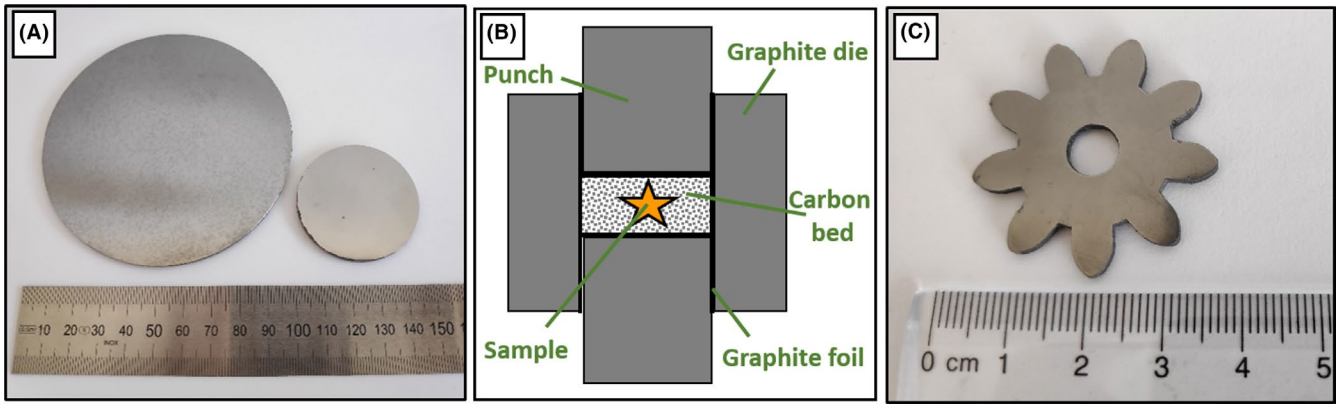

FIGURE 7 A, Dense Cr_2AlC samples with 100 and 45 mm diameter sintered by SPS, (B) scheme of SPS carbon bed approach to sinter complex shapes, and c) highly dense (98.2%) Ti_2AlC gear wheel sintered using SPS carbon bed approach [Color figure can be viewed at wileyonlinelibrary.com]

requirements. The main drawbacks are the high content of secondary phases and eventual milling step.

3.2.3 | Hot-pressing

HP is extensively used to synthesize dense MAX phase samples with high phase purity.[5,127,146] The starting powder is poured into a graphite die and is uniaxially pressed between two graphite punches, followed by a thermal treatment under argon or vacuum. The uniaxial pressure is applied during the whole thermal cycle and the maximum pressure depends on the graphite features, but typically is up to 50 MPa. At temperatures up to 1000°C-1200°C, lower pressures (5-10 MPa) are used to promote the synthesis, whereas higher pressures (up to 50 MPa) should be applied at higher temperatures to promote densification. The maximum temperatures (dwell) are usually between 1200°C and 1700°C, [5,20,144] while heating rate is often up to 20°C/min with isothermal holding times of up to 10 hours at the maximum dwell temperature. Dense samples typically contain large grains (> 10-20 μm) that are oriented perpendicular to the applied pressure. The main advantage is that HP leads to full densification of highly pure MAX phases. However, simple geometries—basically discs up to 4-5 mm in height and 50 mm in diameter—are obtained, requiring a further shaping step prior to use.

3.2.4 | Hot isostatic pressing

HIP leads to highly pure and dense MAX phases as HP, but without any preferential orientation/texturing of the grains due to the isostatic pressure conditions.[49,162] Isotropic microstructures might be beneficial to some specific applications, but the processing and equipment are more complex. The starting powder has to be encapsulated into a suitable glass or metallic container, followed by a thermal treatment under argon at high pressures (100-300 MPa) for several hours. As a result, although the synthesis is possible, HIP is rarely used.

3.2.5 | Spark plasma sintering

Sample preparation is similar to HP but the main difference resides in the thermal cycle. SPS allows faster heating rates (50-200°C/min) and shorter dwell times (<10 minutes) than HP, limiting grain growth.[163] Furthermore, lower temperatures can be used so dense samples are obtained between 1100 and 1400°C.[164,165,166,167] Conventional samples are discs of 4-5 mm in height and 20-30 mm in diameter, although larger samples of 100 mm in diameter are also possible (Figure 7A).' The main advantage of SPS is the full densification of highly pure MAX phases with controlled microstructural features, from fine (<10 μm) to coarse grains. However, the main limitation is again the simple geometry of the produced samples.

3.2.6 | Microwave

MW is a pressureless heating method with high heating rates, a selective heating zone, and direct energy supply and penetration. It is the least explored process of SSR methods, although reported for V_2AlC,[168] Cr_2AlC,[169] Ti_2AlN,[166] Ti_2AlC,[170] Ti_3AlC_2,[171] Ti_2SC,[172], and Ti_3SiC_2.[173,174] Starting precursors are heated under argon atmosphere with heating rates up to 200°C/min, maximum temperatures between 850°C and 1480°C,[170,173] and dwell times up to 30 minutes.[168,171] The reduction of the sintering temperature is associated with the enhanced diffusion of species by their interaction with the microwaves, and the reported decrease of the activation energy, 233 KJ/mol for the formation of Ti_3SiC_2.[174] The synthesized

pellets exhibit high purity, with values up to 97.5%,[171] and grain size in the range between 1 and 10 μm.[169,173] Synthesized pellets are typically porous, although relative densities up to 95% have been reported for Ti_3SiC_2 doped with aluminum.[173] As a consequence, a milling step is added to obtain powders. The advantages are the high purity, short thermal cycles, simplicity, energy and cost saving, and reduction of maximal temperature. However, MW presents some limitations in synthesizing large samples due to temperature gradients.

3.3 | Molten processes

Reactive melt infiltration (RMI) and molten salt (MS) are categorized as molten processes because a liquid phase is involved. Perhaps, RMI and MS are not the most attractive methods to synthesize some MAX phase ceramics for the fundamental studies, but they might contribute substantially to the processing of complex components and synthesis of MAX phase powders.

3.3.1 | Reactive melt Infiltration

RMI is based on the infiltration of a molten metal into a porous preform, followed by their reaction to synthesize the desired material. This method is extensively used for the processing of SiC/SiC and C/SiC composites, where a preform based on SiC or C fibers and a porous carbon matrix is infiltrated with molten silicon at temperatures of 1450°C or higher.[175] This strategy has been also used to synthesize Ti_3SiC_2,[176,177,178] Ti_3AlC_2,[179] and Ti_2SnC,[180] through the infiltration and further reaction of molten silicon, aluminum and tin, respectively. First the porous preform is produced, where compositions such as TiC_x ($0.5 > x > 1$), TiC/C, TiC/TiO_2 or TiC/Ti have been reported.[176,177,178,179,180] Then, the porous preforms are infiltrated with the molten metal at high temperatures under argon atmosphere. Silicon is infiltrated at 1500°C-1600°C, while aluminum and tin required lower temperatures, >1000°C and > 500°C, respectively. However, higher temperatures around 1400°C and 1200°C are needed to promote the synthesis reaction of Ti_3AlC_2 and Ti_2SnC, respectively. Samples with relative densities around 90%–95% can be achieved, but the yield is commonly low due to the presence of carbides, unreacted metal, and intermetallics. Furthermore, RMI has been also used to develop CMCs based on MAX phases, in particular Ti_3SiC_2 reinforced with SiC particle or carbon fibers.[181,182]

3.3.2 | Molten salt

MS is a synthesis method at high temperature where reactions and diffusion of ions and cations are assisted by a liquid phase, precisely a molten salt. Diffusion is enhanced in a liquid media in comparison to a solid-state reaction, thus synthesis temperatures can be lowered, although they are restricted by the evaporation of the salt. Processing is relatively simple, and it involves mixing the precursors with salt, followed by cold pressing to form pellets. An excess of "A" element, up to 20 at.%, is typically added to counter losses. Common salts typically include NaCl or a combination of NaCl and KCl. Pellets are then placed in a crucible and heated to temperatures around 1300°C under argon atmosphere to avoid oxidation. Maximum temperature depends on the chosen system, with values around 1000°C-1200°C for Cr_2AlC,[183] 1000°C for Ti_2AlC,[184] 1200°C-1300°C for Ti_3AlC_2,[184] 1200°C for Ti_3SiC_2,[185] and 1050°C for V_2AlC (although an additional annealing step at 1400°C increases phase purity)[186]. After cooling, the pellets are washed in hot water to remove the residual salt and filtered to obtain loose powders. The purity of powders is high (>95 wt%) but secondary phases and salt residues are difficult to fully eliminate. Particle size depends on the precursors, precursors to salt ratio, and thermal treatment, but it ranges between ~100 nm and ~10 μm. The precursors to salt ratio is typically 1:1, but different ratios allow controlling the morphology and particle size of the synthesized MAX phase powders.[187] Recently, a new process named Molten Salt Shielded Synthesis (MS3) has been reported,[188,189] increasing the potential of the MS method. MS3 is based on the encapsulation of the pellets in a salt, for example KBr, enabling synthesis in air instead of argon. The salt encapsulation has to be gas tight to prevent oxidation of the precursors until melting of the salt. Once the salt is molten, oxidation is avoided because the pellet is completely immersed in the molten salt. MS3 process has been demonstrated for different MAX phases, such as Ti_3SiC_2, Ti_2AlN, Ti_2AlC, Ti_3AlC_2, and V_2AlC as well as MoAlB and Cr_2AlB_2.[188,190,191]

In addition, MAX phases can be synthesized by an electrochemical process based on MS. First a mixture of oxides, such as $Cr_2O_3/Al_2O_3/C$ or $TiO_2/Al_2O_3/C$ for Cr_2AlC and Ti_3AlC_2, respectively, is consolidated at high temperature.[192,193] This pellet acts as cathode, meanwhile graphite bars are the anode. These electrodes are introduced in a molten salt (ie $CaCl_2$) at high temperature, which acts as the electrolyte, and a constant voltage of approximately 3V is applied. An electrochemical reaction occurs, forming a highly dense MAX phase pellet with grain size around 10-15 μm. Furthermore, the MS process can be used to synthesize novel MAX phases through the replacement of the "A" element in a molten salt media. Nb_2CuC and $Ti_2(Al_xCu_{1-x})N$ have been synthesized from Nb_2AlC and Ti_2AlN powders using $CuCl_2$ or CuI salt at 600°C for 7h in argon atmosphere.[194]

MS3 is simple, easy, cheap, and scalable (Figure 6). In addition, it does not require any specific equipment, since a

conventional open furnace with a maximum operating temperature of 1300°C is enough. Furthermore, synthesis takes place at intermediate temperatures (900°C-1300°C) and does not require any milling step to obtain powders. The grain size can be controlled and the process is versatile since electrochemical reactions using cheap oxides can be used and novel MAX phases can be synthesized. The main disadvantages are the high content of water that is required for the washing step, and the impossibility to fully densify bulk samples in a single step.

4 | STRUCTURES

Most of the studies to date have focused on bulk specimens with simple geometries sintered by HP or SPS, and thin films obtained using PVD techniques. These specimens are essential for fundamental studies, but practical applications demand components of different geometries. Herein, the processing of different structures is relatively limited. In this section processing of dense samples, ceramic matrix composites, foams with different porosity levels, coatings, and near net-shape processing are summarized.

4.1 | Dense bulk samples

Full densification of MAX phases cannot be achieved by PLS—maximum relative densities around 90%. Thus, pressure-assisted sintering techniques are required, limiting the sample geometry mostly to discs and plates. Dense bulk specimens with high purity produced by SPS typically have fine grains (around 3-15 μm) while those produced by HP have elongated coarse grains (>15 μm). Most of the time, reactive sintering (synthesis and sintering in the same thermal cycle) is performed due to simplicity and precise control of purity. However, sintering of pre-reacted MAX phase powders by SPS often leads to a better control of the microstructure. For example, Badie et al have recently synthesized submicron Ti_2AlC powders by MS3, followed by densification by SPS at 1200°C for 10 minutes to produce dense Ti_2AlC with an average grain size below 1 μm, which is the finest microstructure reported for a dense MAX phase to date.[195]

Pressure assists densification but can promote texturing, where basal planes of grains are oriented perpendicular to the applied force. As expected, texturing is mostly observed in HPed samples due to the long sintering times and coarse microstructure, meanwhile SPSed samples present practically isotropic microstructures or slight texturing. Texturing can be magnified to tailor the microstructure and properties. MAX phase powders were slip casted and oriented under strong magnetic fields (around 10-12 T), followed by SPS. Lotgering orientation factors for the top and side surfaces in the range of 0.6 to 0.7 have been reported for Ti_3SiC_2, Nb_4AlC_3, and Ti_3AlC_2.[61,34,196,197] Another approach is referenced as edge-free spark plasma sintering (EFSPS) and is based on the plastic deformation near the brittle-to-plastic transition temperature.[198] In this case, a dense MAX phase disc with a smaller diameter than the graphite die was heated in a SPS system under low pressure near to the brittle-to-plastic temperature. At this temperature high pressure was applied, deforming the sample until its diameter was equal to the inner graphite die and promoting texturing.[198] Uniaxial pressure usually precludes the sintering of complex structures in SPS, but a recent strategy based on a carbon bed leads to sinter near net-shapes.[199,200] The green sample with a complex structure was surrounded completely by graphite powders, which was placed in a graphite die and between two graphite punches (Figure 7B,C). Then, a conventional SPS cycle was run, where mechanical load was transferred to the sample to produce pseudo-isostatic conditions.[199,200] This strategy has been performed on a Ti_2AlC gear wheel processed by injection molding and sintering at 1350°C and 50 MPa of uniaxial pressure (Figure 7B,C).[201] The gear wheel had a relative density of 98.2%, while only 89.6% was achieved by pressureless sintering at the same temperature.

4.2 | MAX phase composites

MAX phases have been reinforced with ceramic particles to improve their mechanical and tribological performance, and they have also been used as reinforced phase in metallic and polymeric matrices. In general, the precursors are mixed in precise quantities to attain the maximum MAX phase yield, minimizing the content of carbides or nitrides. However, the content of these secondary phases can be controlled through the quantities of the starting powders to develop Ceramic Matrix Composites (CMCs). Ti_3SiC_2 composites containing 30 vol% of SiC particles or 30 vol% of TiC particles were sintered by HIP at temperatures up to 1600°C modifying the amounts of TiH_2, α-SiC, and graphite.[162] Similar strategy was used by Tian et al,[202] where Ti, Si, and TiC were used as starting powders to synthesize Ti_3SiC_2 using SPS at 1400°C, as well as to develop Ti_3SiC_2/TiC composites through the addition of excess TiC. The incorporation of TiC particles increases the hardness from 5 GPa (nominally pure Ti_3SiC_2) to approx. 11 GPa (Ti_3SiC_2 containing 40 vol% TiC). A similar trend was observed for the flexural strength, which increased from ~350 MPa to ~575 MPa with the incorporation up to 40 vol% TiC.[202] Ti_3SiC_2 composites containing TiB_2 and TiC particles were also sintered using HP at 1500°C for 2 hours through the adjustment of the starting TiH_2, Si, graphite, and B_4C precursors.[203] In this work, oxidation response up to 1200°C was improved with the incorporation of TiB_2 particles. Cr_2AlC containing up to 20 vol% Al_2O_3

particles were processed by in-situ reaction of Cr_3C_2, Cr, Al, and Cr_2O_3 powders in HP at 1400°C.[204] Hardness and flexural strength increase continuously with the alumina content, meanwhile the fracture toughness increases with contents up to 11 vol% Al_2O_3 followed by a decrease for higher alumina contents. This strategy is simple and controls properly the second phase content, but unfortunately does not tailor the morphology of the particles.

Control of morphology can only be attained through the incorporation and dispersion of the second phase into the MAX phase powders, followed by consolidation at high temperature. This was the case for developing Ti_3SiC_2 reinforced with cubic-BN,[205] and MAX phase composites reinforced Al_2O_3 and SiC fibers. Carbon fibers react with MAX phases—at least with Ti_3SiC_2, Ti_2AlC, Ti_3AlC_2, and Cr_2AlC- so the composites will contain a strong reaction zone at the matrix/fiber interface that grows and consumes the fibers at high temperature. Nevertheless, Ti_3SiC_2 reinforced with C fibers has been processed,[206,207] showing a reaction zone at the interface that was minimized through the fast sintering using SPS.[207] Reactions also take place between Ti_2AlC and Ti_3AlC_2 with SiC fibers, forming TiC and Ti-Al compounds.[208] However, the reaction is hindered using a titanium barrier layer between the commercial SiC fibers and the Ti_3AlC_2 powders, enhancing the flexural strength and promoting a non-catastrophic fracture behavior.[209] No reactions have been reported for Ti_3SiC_2 and Cr_2AlC with SiC fibers at high temperature,[116,208] as well as for Ti_2AlC, Ti_3AlC_2, and Cr_2AlC with Al_2O_3 fibers.[210,211] In the case of Ti_3SiC_2 reinforced with SiC fibers or SiC whiskers, the creep resistance at temperatures up to 1300°C was improved up to two orders of magnitude.[212,213] Furthermore, addition of 10wt% of short SiC fibers into Cr_2AlC enhanced the tribological response, specifically a reduction of 20% in the friction coefficient and up to 80% in the wear rate.[116]

MAX phases have also been added into metallic matrices to improve some properties. For example, Cu/Ti_3SiC_2 composites were processed by powder metallurgy to develop a new electrofriction material with a self-lubricated response.[214] Copper was also mixed with Ti_3AlC_2 particles and consolidated by HP, and the composites present

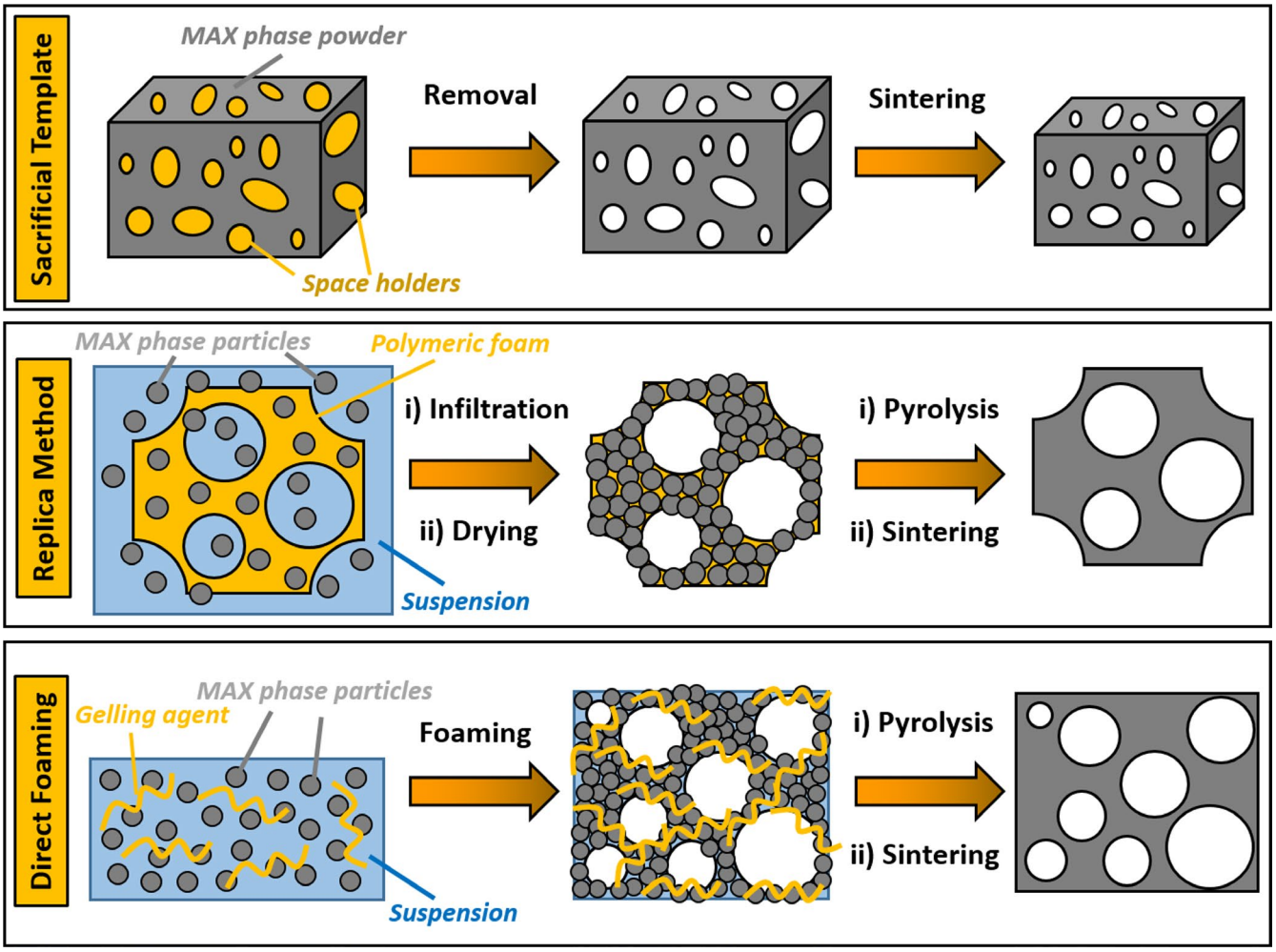

FIGURE 8 Scheme of space holder template, replica method, and direct foaming for the production of MAX phase porous architectures [Color figure can be viewed at wileyonlinelibrary.com]

superior flexural strength than copper without a remarkable loss of fracture toughness.[215] In addition, Cr_2AlC particles were used to tailor the electrical performance of copper, in particular to improve the arc erosion ability.[216] Aluminum has been also reinforced with Ti_3AlC_2 particles, increasing the yield stress up to 100% over the temperature range of 20°C-500°C.[217] Mg-alloy (AZ91D) composites containing Ti_2AlC particles were fabricated by stir casting technology to increase the yield strength, Vickers hardness, ultimate compressive strength, and elastic modulus.[218] Another alternative is to process a highly porous MAX phase structure (porosity around 40-60 vol%), which can then be infiltrated with a molten metal at high temperature. Mg/Ti_2AlC,[219] Al alloy/Ti_2AlC,[220] NiTi/Ti_3SiC_2, and NiTi/Ti_2AlC,[221] were processed using this method. The Mg/Ti_2AlC composites showed a reversible, reproducible, hysteretic stress-strain loops during uniaxial cyclic compression tests, as well as a superior ultimate compressive (700 MPa) and tensile strength (380 MPa) in comparison to other Mg composites.[219]

4.3 | Porous architectures

MAX phase porous structures present an excellent combination of properties such as low density, good corrosion and oxidation resistance, high surface area, machinability, superior mechanical properties, and electrical conductivity. Content and size of the porosity can be precisely controlled by the processing route, which are categorized in three main groups: sacrificial template, replica method, and direct foaming (Figure 8).[222] Additionally, the incomplete densification obviously entails a porous material, but in this case the size of the porosity cannot be controlled (Figure 9).[223,224]

4.3.1 | Sacrificial template

It is the most used process and is based on mixing MAX phase powders with a disposable material (referenced as space holder) with well-defined particle size (Figure 9). The mixture is pressed to obtain pellets, followed by removal of the space holders to produce green bodies with defined porosity. Removal of the space holders can be carried out by a washing process, ie NaCl and sugar, or by pyrolysis. Afterwards, porous green bodies are sintered under pressureless conditions. Ti_2AlC foams have been processed by sacrificial template using NaCl as space holder, obtaining porosities between 10 and 80 vol. % and pore sizes between 42 to 1000 μm.[225,226,227,228] The same method was successfully used to develop Ti_3SiC_2 foams with 60 vol% porosity and pore size up to 1mm, although some degradation of Ti_3SiC_2 occurred during thermal treatment. In addition, Ti_3SiC_2 foams were also developed using NaCl as space holder, but in this case Ti, Si, and graphite powders were used as precursors instead Ti_3SiC_2 powders. During the thermal treatment Ti_3SiC_2 was formed but the precise control of the porosity was more complex and depended on the content and size of the template.[229] Furthermore, Cr_2AlC foams with porosities between 35 and 75 vol% and sizes between 90 and 400 μm were performed using NH_4HCO_3 as space holder.[230] The Cr_2AlC foams had a good oxidation response up to 1300°C and excellent compressive strength at room temperature in comparison to other ceramic foams. Interestingly, the compressive strength of Cr_2AlC foams increased after oxidation at 1200°C due to the formation of a dense and adherent alumina layer. Furthermore, creep resistance of Cr_2AlC foams containing 53 vol% porosity was tested in air at temperatures up to 1200°C and compared to dense samples.[42] Dislocation motion was identified as the probable mechanism, and,

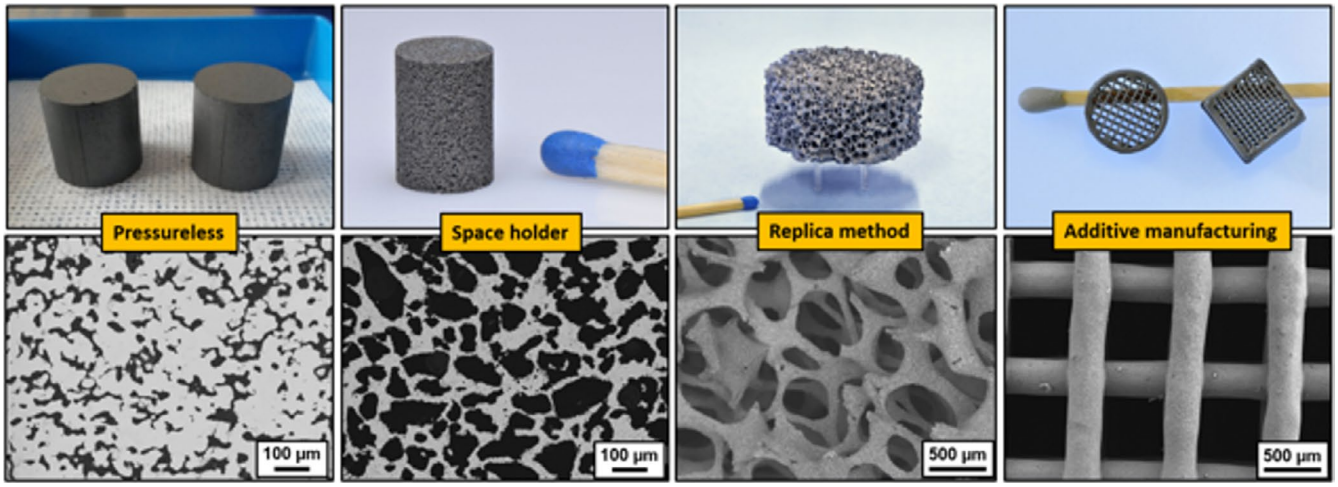

FIGURE 9 Photographs and SEM micrographs of Cr_2AlC porous structures processed by pressureless sintering, space holder technique, replica method, and additive manufacturing [Color figure can be viewed at wileyonlinelibrary.com]

surprisingly, creep rate was lower for the foams under some conditions, which was attributed to the oxide scale. The effect of this alumina scale on the mechanical behavior at room and high temperature (298-1398 K) was further evaluated by Araki et al[231] The alumina scale prevents outward crack propagation from the volume, but this positive effect depends on the thickness of the scale, that is, <2.5 and <5.0 μm at 273 and 1398 K, respectively. Additionally, life time estimation of these Cr_2AlC foams was calculated according to the operating temperature and scale thickness, that is, 10^5 hours at 1100 and 10^3 hours at 1300°C.

4.3.2 | Replica method

It is based on the infiltration of a ceramic suspension into a polymeric foam (Figure 9). The ceramic suspension has to present a shear thinning response, which means low viscosity under high shear forces, to facilitate the infiltration, and high viscosity in absence of forces to remain into the foam. After infiltration, the polymeric foam is pyrolyzed, followed by pressureless sintering of the porous structure. The first MAX phase foam by replica method was reported by Sun et al[125] using Ti_3AlC_2 powders, poly-acrylic acid as dispersant, colloidal silica as binder and commercial polyurethane sponges with 120 ppi (pores per inch). The reticulated structures presented 80 vol% of open porosity with well-defined and homogeneous porosity after removing the sponge template. Ti_2AlC foams were also performed using commercial MAX phase powders, poly(ethylenglycol) as plasticizer and binder, Dispex GA40 as anti-settling agent, methyl-cellulose as thickening agent, and commercial polyurethane foams of 10 ppi.[232] Two infiltration processes decreased the number of defects in the struts, increasing the mechanical stability of the final reticulated structures. In addition, Cr_2AlC foams were processed by replica method using Cr_2AlC powder, polyacrilic acid as dispersant, methyl-cellulose as thickener and commercial polyurethane foams with 20 and 30 ppi.[233] Two infiltration processes were also required to increase the density of the struts and achieve good mechanical stability.

4.3.3 | Direct foaming

Gel casting of Ti_2AlC has been reported to obtain foams with porosities higher than 90%.[234,235] Gel casting is based on the preparation of a suspension containing a gelling agent such as agarose (Figure 9). Foaming is carried out through agitation (or blowing air), followed by pouring the foamed suspension into a cold mold to form a strong and connected network. The solid is dried, organics are pyrolyzed, and the foam is sintered under argon. Ti_2AlC foams presented porosities up to 93 vol% with high degree of interconnectivity, an average cell size from 335 to 615 μm, and an average cell window size between 72 and 162 μm.[234]

4.3.4 | Additive manufacturing

Another alternative to develop MAX phase structures with controlled porosity is to use additive manufacturing (AM) (Figure 9). This approach can produce bimodal porosity, which is based on millimeter range channels between struts, and micro-porosity within struts due to incomplete densification. Well-defined, complex structures have been recently reported for Ti_2AlC and Cr_2AlC,[126,236]. As with the replica method and direct foaming, control of rheological properties is crucial. Ti_2AlC inks were developed using commercial powders and polyethylene glycol or polyvinyl alcohol as organic binders in water and extruded by direct ink writing. The porous Ti_2AlC lattices were sintered at 1400°C in argon, resulting in total porosities between 44 and 63 vol%, and mechanical strengths ranging between 43 and 83 MPa.[236] Regarding the 3D porous Cr_2AlC architectures, MAX phase powders were mixed with polyethylenimine as dispersant, hydroxypropyl methylcellulose as thickening agent, and ammonium polyacrylate as flocculant.[126] The resulting ink was extruded by robocasting, followed by a drying process and consolidation by SPS under pressureless conditions. The 3D structures present a porosity between 60% and 64% (Figure 9), with excellent mechanical performance, high electrical conductivity, tailored heat dissipation and good thermal cycling resistance.

4.4 | Coatings

Highly pure and dense thin films can be deposited by PVD at fairly low temperatures, which certainly might be determinant to coat sensible substrates. The thickness of these films ranges commonly between few nm to ~50 μm, but for thicker coatings thermal spray technologies are preferred. Briefly, thermal spray deposition is based on the ejection and acceleration of heated and/or molten particles towards a substrate. Coatings of up to some millimeters can be obtained. High gas temperatures (> 10.000°C) are typically required to accelerate (100-500 m/s) the particles and to heat/melt them. However, MAX phases might oxidize and degrade due to these high gas temperatures and their inherent incongruent melting, even under the low particle flight-times ($<10^{-2}$ s). This was the case during the deposition of commercial Ti_2AlC powders (initial purity of 68.3%) by plasma spray, where coatings were underdense and presented only 26% Ti_2AlC purity.[237] One alternative was to use high gas temperature to synthesize MAX phases in-situ during spraying.

Feedstock composed of Ti, Si, and graphite powders were deposited by plasma spray, but the very short time (~ 10^{-4} s) limited the Ti_3SiC_2 formation, achieving purities lower than 20%.[238] Similar results were obtained after the deposition of Cr, Al, and graphite powders by plasma spray, where the yield of Cr_2AlC was only 1.6 wt%, which increased up to 23.7% after an annealing process at 800°C. [239]

The best alternative is to avoid high temperatures during spraying, such as High velocity oxy fuel (HVOF) and cold spray (CS), that use lower gas temperatures, but higher velocities to provide enough kinetic energy to the particles. Gas temperatures are strongly reduced to 2000-3000°C and 300-1000°C for HVOF and CS, respectively, whereas the particle velocity ranges from 400 to 700 m/s and 700 to 900 m/s. Highly dense, 200 μm thick and adherent Ti_2AlC coatings were deposited on Inconel substrates by kerosene-fueled HVOF, although purity was only 53 wt%.[240] Comparable results were reported for other HVOF depositions using commercial Ti_2AlC powders, where highly dense coatings that were 100-200 μm thick contained TiC and Ti_xAl_y particles.[241,242,243] In spite of the high density, thickness, and adhesion of the HVOF coatings, the gas temperature still causes the MAX phases to decompose into carbides and intermetallics. The degree of degradation of MAX phases is decreased when powders are deposited by CS. Most ceramics cannot be deposited by CS, but the shear response and high deformability of MAX phases allows for this possibility (Panel A). Approx. 90 μm thick Ti_2AlC coatings with high density and good adhesion were deposited onto Zircaloy-4 substrates.[244] In general, purity is maintained by CS, although coatings typically have inter-splat cracks.[245,246] Highly pure Cr_2AlC powders were deposited by CS (Figure 10 A,B), obtaining highly pure coatings (>98% by Rietveld) with preferentially oriented particles.[247] As for other MAX phase coatings processed by CS, some inter-splat cracks were detected, leading to a final relative density up to 91%. CS is certainly a good technique to develop MAX phase coatings since purity is kept and large thicknesses and relatively high densities can be attained. However, optimization of the powder features is required to increase the density of coatings.

High velocity atmospheric plasma spray (HV-APS) and liquid plasma spray (LPS) have been used to deposit Cr_2AlC and Ti_3AlC_2.[248,249] Cr_2AlC coatings with thicknesses up to 100 μm and relative densities up to 93% were deposited on stainless steel and Inconel 738 by HV-APS (Figure 10 C). Coatings exhibited good adhesion, but Cr_2AlC was partially decomposed. Additionally, Cr_2AlC coatings were used as bond-coat, between an Inconel substrate and a conventional porous YSZ TBC layer. The Inconel/Cr_2AlC/YSZ system was tested in a burner rig at 1400°C (surface temperature) and survived 745 cycles, indicating that Cr_2AlC has a high potential as bond-coat.[248] Regarding the deposition of Ti_3AlC_2 powders by LPS,[249] coatings were 10-20 μm thick with high density and purity despite an expected temperature higher than 2200 K during deposition. The solvent and the pH play a determinant role, but more investigation is required to confirm and improve these promising results. Finally, electrophoretic deposition (EPD) has briefly been explored to develop MAX phase coatings, however, porosity issues were observed in the coatings. $Ti_3Si(Al)C_2$ powders were deposited at 3V on indium-tin-oxide substrates from a suspension with 1 vol% solid loading at pH 9 without any dispersant.[250] The coatings were not dense and exhibited a (00l) preferred orientation. In addition, porous Ti_3SiC_2 coatings were deposited by EPD at 10V using a 4.3 wt% solid loading at pH 9.[251] Afterwards, the thin coating was rapidly densified using a 3D printing laser, but only some Ti_3SiC_2 remains after sintering.

4.5 | Near net shaping

Different approaches, with respect to the complexity of the structure, have been performed to produce near net shape components. Surprisingly, the number of investigations is rather low, which has reduced the interest of potential industrial partners.

Slip casting is a simple and inexpensive method to manufacture large and thin walled complex parts. The first investigation was performed by Ansell Healthcare and Drexel University to make latex products.[20] Subsequently, Sun et al investigated the

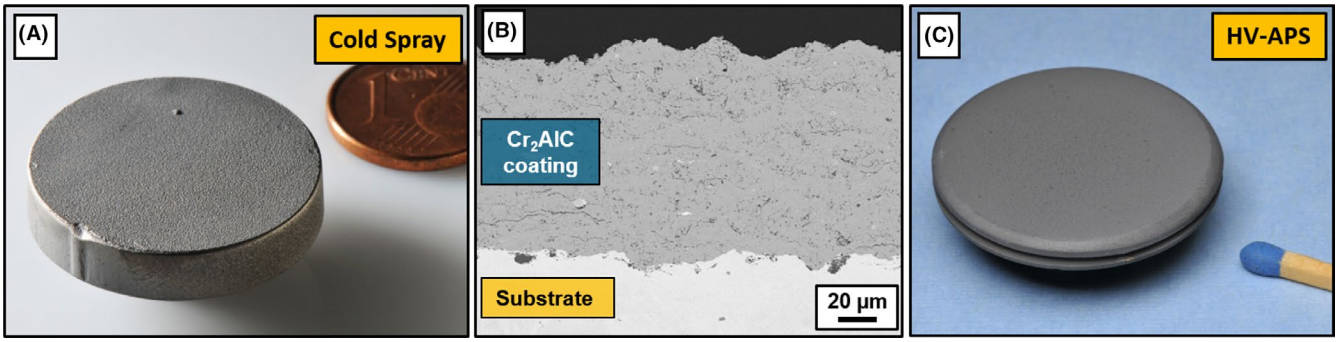

FIGURE 10 A, photograph of Cr_2AlC coating on Inconel 738 by Cold Spray, (B) cross section of Cr_2AlC coating by CS, (C) photograph of the Cr_2AlC coating deposited by high velocity—atmospheric plasma spray [Color figure can be viewed at wileyonlinelibrary.com]

rheological properties, revealing that Ti_3AlC_2 suspensions with 2.0 dwb% PAA at pH 5 present an excellent stability and a characteristic Newtonian behavior.[252] The relative densities of green bodies were 61% and PLS samples was 96%. Ti_3AlC_2 particles can be dispersed in basic pH, particularly at pH 10 and using 1 wt% of Arabic gum as dispersant.[253] The green compacts were densified at 1450°C for 90 minutes using an Al_4C_3 powder bed, achieving 95.3% relative density and a low content of impurities. Recently, Ti_3SiC_2 tubes have been processed by slip casting as a proof of concept for nuclear fuel cladding.[254] The suspension contained 49.5% dry weight basis (dwb) Ti_3SiC_2, 46% dwb water, 4% dwb polyethyleneimine, and 0.5% dwb. methylcellulose, and it was sintered at 1450°C for 2h under vacuum. The sintered tubes had a relative density of 89% with some silicon loss at the outer edges.

Injection molding is widely used in industry to shape small items due to the high precision, simplicity, velocity and low cost.[255] The first step is the preparation of the feedstock, which is a mixture of powders, wax, thermoplastic binder, and additives. The feedstock is injected into a mold at temperatures around 100°C-200°C, and the near net shapes are debinded first in a non-polar solvent to remove the wax, and then in an oven to remove the rest of the binders. Finally, the components are sintered. Commercial Ti_2AlC and Ti_3SiC_2 powders were mixed with paraffin 65 as wax, to ensure the mechanical stability and stearic acid to lubricate.[256] Feedstocks contained 62 vol% of solid content and 38 vol% of the binder system, and were injected into a gear wheel mold with a flow rate of 15 cm^3/s, injection pressure of 1150 bars, and injection and mold temperatures of 175°C and 90°C, respectively (Figure 7C). Ti_2AlC-Al composites have been also processes using commercial Ti_2AlC powders.[257] The feedstock contains 83 wt% of hydrophobized Ti_2AlC, 15 wt% of paraffin and 2 wt% of carnauba wax, and was injected into building block molds with dimensions of 4.6 mm × 1.5 mm × 1.5 mm. Afterwards, the Ti_2AlC building blocks were sintered in argon at 1350°C, and jointed to brick-and-mortar structures using aluminum as filler.

AM is an excellent approach for small samples with a high degree of complexity, although presents two main challenges for MAX phases: full densification of the 3D structure—as in general for ceramics—and the inherent incongruent melting. As a result, AM techniques that utilize melting, such as selective laser melting, should be avoided to retain phase purity. One alternative might use the focalized high temperature to synthesize MAX phases, but the extremely fast kinetics reduce the phase yield.[258] The first publication was reported in 2002 by Sun et al,[259] where fully dense (> 99%) and complex Ti_3SiC_2 structures were obtained by a three-stage fabrication process, based on 3D layered printing, cold isostatic pressing and sintering. The green parts were built by deposition of Ti_3SiC_2 powder by binder spray layer, using layers of ~90 μm and ~180 μm thick. In spite of this promising outcome, the most used approach for MAX phases so far is the combination of 3D printing of a porous carbide, followed by liquid silicon infiltration or reactive melting infiltration with aluminum to synthesize Ti_3SiC_2 and Ti_3AlC_2, respectively.[176,260,261,262] Densities are high, but the main problem is the low yield of the synthesis reaction that ranges between 50 and 90 wt%. A similar concept was performed to produce gears by laminated object manufacturing.[263] Tapes with thickness of approx. 100 μm, composed of TiC and SiC, were processed by tape casting followed by drying and lamination. Afterward, green tapes were processed via Laminated Object Manufacturing to fabricate a 3D gear structure, consolidated at 1600°C, and infiltrated with silicon at 1450°C. The gears were fully dense but Ti_3SiC_2 coexisted with other phases such as $TiSi_2$. The best alternative to achieve high purity is to manufacture 3D structures using MAX phase powders, followed by their consolidation at high temperature. Robocasting and direct ink writing—based on the same principle - have been used to produce complex 3D structures based on Cr_2AlC (Figure 9) and Ti_2AlC, respectively.[126,236] The processing was described above in Section 4.3 (porous architectures).

5 | POTENTIAL APPLICATIONS

In the late 1990s, Kanthal Corp. licensed the MAX technology from Drexel University and developed Ti_2AlC heating elements and considered other potential applications.[20] These heating elements were cycled from room temperature to 1350°C approximately 8000 times, showing a very stable behavior due to a protective, adherent oxide scale.[64] Likewise, Ti_2AlC was proposed as nozzles in gas burners, showing an outstanding response in a corrosive environment (not described) that severely degraded the steel nozzles.[20] However, to the best knowledge of the author, these products are not currently in the market. The only current product in operation is Cr_2AlC pantographs for electric high-speed trains in China, which have successfully replaced carbon-based ones. Almost 25 years have passed since the rebirth of MAX phases (1996), which is a realistic time to find some applications for the market. Among the different reasons for the lack of commercial use, the most determinants are: i) lack of commercial powders with high purity at affordable costs, ii) complexity of this large family of materials and large number of new compositions (> 150 MAX phases), and iii) large period of time (ie 20-30 years) required to qualify products in strategic for nuclear or aerospace applications.

5.1 | High-temperature structural material

The most likely potential application for Al_2O_3 scale-forming MAX phases is as components that operate under

aggressive environments at temperatures between 1100°C and 1400°C over long period of times. In addition to heating elements and gas nozzles, Ti_2AlC, Ti_3AlC_2 and Cr_2AlC are potential candidates to replace Ni/Co superalloys in the hottest part of a gas turbine engine to enable operation at higher temperatures and thereby increase efficiency. Ni/Co superalloys have maximum operating temperature around 1100°C-1150°C, which could be increased by ~100°C using MAX phases. Combustor liners, blades and vanes withstand temperatures above 1600°C, oxidizing atmospheres, entry of corrosive particles such as CMAS and foreign objects, and high thermal and mechanical stresses. Superalloys are protected from these conditions by TBCs, which are based on an external porous oxide layer and an intermediate bond-coat.[264] MAX phases have an excellent CTE match (Figure 5) with standard TBC materials and the thermally grown oxide (TGO) α-Al_2O_3 at high temperature. Consequently, the thermal stresses are reduced by nearly an order of magnitude compared to conventional high temperature alloys (CMSX-4, CMSX-10, Rene 80 or Inconel 738), [53,94,95] which can extend the life of the whole system. Additionally, bond-coats are not any longer required due to the strong adhesion, compatibility and formation of TGO, simplifying the processing.[73,94,95] Furthermore, Ni/Co superalloys are composed of and typically doped with strategic elements that have limited supplies and/or under serious threat, that can also be toxic to the environment and human health. Meanwhile, elements such as Ti, Al, and C that compose MAX phases are abundant in high quantities, nontoxic, and cheap.

5.2 | High temperature coatings

MAX phase coatings are being considered as protective coatings for refractory alloys and as bond-coat layers in TBC systems. In both applications, CTE is critical to reducing stresses and avoiding spallation of the coating. Cr_2AlC is more suitable for metallic systems due to the larger CTE (12.0-13.3 $\times 10^{-6}$ K^{-1}), meanwhile Ti_2AlC and Ti_3AlC_2 (8.2-9.0 $\times 10^{-6}$ K^{-1}) match better with TBC compounds. For example, advanced turbine disks can be protected against Type I and II Low Temperature Hot salt Corrosion (LTHC).[68,69] Cr_2AlC coatings deposited on a low γ'solvus and a high refractory content alloy—referenced as LSHR and developed at NASA—prevented hot corrosion pitting and improved the low cycle fatigue resistance up to 90%. Recently, Cr_2AlC bond-coats have been deposited on Inconel 738 substrates, followed by deposition of a porous yttria-stabilized zirconia as external TBC.[248] The system was tested under thermal loading conditions similar to a gas turbine environment, achieving surface and substrate temperatures of 1400°C and 1050°C, respectively. The system failed after 745 cycles (conventional bond-coat systems under similar conditions around 1000-1200 cycles) mainly for three reasons: (i) open porosity of the Cr_2AlC bond-coat layer, (ii) oxidation of secondary phases, and (iii) inter-diffusion. Furthermore, future challenges to specifically transfer MAX phase as bond-coats are described elsewhere.[248] In this case, Cr_2AlC was tested, but Ti_2AlC presents even more potential because of better CTE match.

5.3 | Nuclear

Phases such as Ti_3SiC_2, Ti_2AlC, Ti_3AlC_2, Cr_2AlC, V_2AlC, Zr_2AlC, Zr_3AlC_2 and Nb_4AlC_3, that combine excellent radiation tolerance with oxidation and corrosion resistance, mechanical properties and chemical stability have attracted considerable attention as potential accident tolerant fuel (ATF) claddings in third-generation light-water reactors (LWRs) and future fourth-generation fission plants. Zirconium alloys fulfill the characteristics to operate as cladding materials in nuclear power plants, but they perform poorly in the event of Loss of Coolant Accidents (LOCAs) as happened in Chernobyl (1986) and Fukushima (2011). MAX phases could replace or coat zirconium alloy claddings due to their superior oxidation and corrosion resistance. For this specific case, dense, highly pure, and nontextured coatings based on MAX phases should be processed at low temperature to avoid damage and/or any modification of the zircaloy substrates. Furthermore, one of the six Generation IV nuclear reactor concepts under development is based on a lead-cooled design.[265] This design is commonly referred as lead-fast reactor, since fast neutrons (>1 MeV) are used for the fission reaction. This high energy neutron spectrum results in higher fuel efficiency, enabling the usage of depleted uranium as nuclear fuel and transmutation of long-lived nuclear waste.[266] The good radiation tolerance, oxidation and corrosion resistance, mechanical stability and excellent compatibility with Pb-alloy coolants of some MAX phases is very promising.[87] Specifically under certain operating conditions most of the nuclear steel grades suffer from liquid metal embrittlement and heavy liquid metal attack (HLM), necessitating the search for alternative materials.[267]

5.4 | Electrical contacts

Ti_3SiC_2 has been proposed as ohmic contacts on 4H-SiC due to its linear current-voltage behavior. Furthermore, Ti_3SiC_2 can easily be processed in a single-step by sputter-deposition of Ti on SiC substrates.[268] This approach puts forward the possibility to directly synthesize oxygen-barrier capping layers after the main contact is deposited, without exposing the

device to air, avoiding potential oxidation, contamination or any need for a cleaning step, thus, increasing the long-term stability of the device. Furthermore, Ti_2AlN has also been considered as ohmic contact for GaN-based devices due to the ohmic behavior with contact resistivity in the range of 10^{-4} $\Omega \cdot cm^2$.[269]

5.5 | Heat exchangers

One more application that has been considered is to use MAX phases as heat exchangers for higher temperatures (~850°C) than conventional metallic systems,[270] where ceramics are the only alternative. Unfortunately, their poor mechanical properties, difficult machinability, low thermal conductivity, and CTE have limited their use. MAX phases can operate at high temperature (up to 1400°C), have better thermal shock response, mechanical properties, chemical stability and machinability than SiC and other advanced ceramics. However, the main limitation is the intermediate thermal conductivity (12 and 60 W $m^{-1}K^{-1}$), which is acceptable, but lower than SiC compounds (up to 125 W $m^{-1}K^{-1}$).

5.6 | Concentrated solar power (CSP)

CSP systems convert solar energy into electric power without greenhouse emission and offer the possibility of thermal energy storage. CSP designs concentrate solar radiation into a receiver using mirrors, and the heat is transported by a heat transfer fluid (HTF) to a steam turbine to produce electricity.[271] As for all the thermal processes, efficiency of energy conversion increases with higher temperatures and combined cycle systems.[272] The temperature of CSP combined cycles should be in the range of 1000-1500 K, and heat is carried by HTFs such as air, molten salts, minerals, or synthetic oils. Other nonoxide ceramics such as SiC and ZrB_2[273,274] have also been proposed as solar receivers due to their higher degradation temperatures.[275] Particularly, porous SiC volumetric receivers have attracted a lot of attention due to the enhancement of heat transfer per unit volume combined with a low drop in pressure.[276] MAX phases have potential in two different CSP sections, the solar receiver and the storage tank. The solar receiver should have excellent oxidation resistance, and features such as high absorptance (α_s) in the ultraviolet-visible-near infrared (UV-vis-NIR) region and low thermal emission in the infrared (IR) region.[277] Unfortunately, not enough research has been performed to confirm the potential of Ti_2AlC and Cr_2AlC for CSP applications.[278] Both MAX phases have excellent resistance to high concentrated flux (527-917 kWm^{-2}), although Ti_2AlC shows higher light scattering due to surface oxidation. The thermal performance of Ti_2AlC and Cr_2AlC varies in the range of 0.56-0.68 and 0.60-0.67, respectively, for the selected flux levels. Regarding the volumetric receivers with open and controlled porosity, MAX phase foams have a high potential due to the low oxidation and the excellent thermal shock resistance in comparison with SiC, but so far they have not been tested. Furthermore, they have potential as structural material for storage tanks because of their excellent compatibility with molten solar salts. K. Van Loo et al have recently reported and tested the compatibility of different MAX phases, SiC grades and reference metallic structural materials with a molten salt (40 wt% KNO_3 and 60 wt% $NaNO_3$) for 1000 hours at 600°C.[86] In this study Cr_2AlC shows a superior corrosion resistance due to the formation of a micrometric-thin and protective layer of Cr_7C_3.

5.7 | Catalysis

catalyst performance has been less explored, but has high potential due to the massive number of compositions and solid solutions in "M", "A", and "X" sites. MAX phases can act both as catalyst and support. Cr_2AlC powders have been tested as solid catalyst to reduce the formation of carbon monoxide in catalytic wet peroxide oxidation (CWPO) processes.[279] The CO concentration in the fenton process reaches a maximum of 6651 mg/Nm^3, which is notably reduced to 187 mg/Nm^3 by the presence of Cr_2AlC, and particularly noteworthy when compared to CO values (2454 mg/Nm^3) of conventional activated carbon-Fe catalysts. Ti_3AlC_2 increases the reversible hydrogen storage properties of MgH_2,[280] as well as the oxidative dehydrogenation of n-butane.[281] Furthermore, Ti_3SiC_2, Ti_2AlC, and Ti_3AlC_2 show excellent chemoselectivity with 100% selectivity for the hydrogenation of organic compounds with low contents of Palladium (0.0005 wt%).[282] As catalyst substrate, reticulated porous Ti_3AlC_2 was coated with nanocrystalline CeO_2 for gas exhaust devices.[125] Around 50%-90% of the total emission of hydrocarbons from modern cars with three-way catalysts are released during the cold start of the engine when the catalyst activity is still low. One solution is the preliminary electric heating of the system, limiting the use of ceramic foams but opening the possibility of MAX phases due to their good electrical conductivity, thermal stability, and high mechanical strength.

5.8 | Joining

Joining is a critical technology to manufacture large, complex assemblies through the controlled integration of smaller, simpler parts. Joining is particularly challenging for ceramic

components, such as monolithic SiC and SiC/SiC composites, as well as for the integration of ceramic parts into metallic systems. Among the different methods, most of them use an inert or reactive filler materials at the interface. In the particular case of MAX phases, they can be directly joined by solid-state diffusion without the incorporation of any filler compound. Ti_3SiC_2/Ti_3SiC_2, Ti_3AlC_2/Ti_3AlC_2, and Ti_3SiC_2/Ti_3AlC_2 have been joined at temperatures <1300°C and pressures between 10-30 MPa.[283,284] The joining is strong and attributed to the interdiffusion of Si and Al at the interface. MAX phase tapes—mainly Ti_3SiC_2—with thicknesses between 30 and 100 μm have been proposed as a filler material to join SiC at high temperatures. At temperatures around 1300°C, the joining is successful with bending strength of ~80 MPa due to a dense interface.[285] However, at higher temperatures, 1500°C-1900°C,[286] the strength increases to almost 170 MPa due to a chemical reaction at the interface and the partial or complete decomposition of Ti_3SiC_2.[287,288] Decomposition might promote a strong joint between SiC parts since a uniform, strong, and dense TiC/SiC interface without cracks is obtained.[289] The residual thermal stress of SiC/Ti_3SiC_2/SiC joints were also calculated by finite element analysis, showing strong stress reduction and high bending strength (157 MPa) when the system is post-annealed at 900°C.[290]

MAX phases can be also joined to metallic components, although some reactions at the interfaces have been detected. Cr_2AlC coupons were vacuum diffusion bonded to an advanced turbine disk alloy at 1100°C.[291] The interface revealed an inner diffusion zone of approx. 10 μm of β-Ni(Co)Al, decorated with γ´$(Ni,Co)_3Al$, Ta(Ti,Nb)C, and $W(Cr,Mo)_3B_2$ precipitates. On the Cr_2AlC side, a porous Cr_7C_3 layer of ~40 μm was detected, whereas on the superalloy side, enhanced carbide precipitation developed over a depth of ~80 μm. Dense Cr_2AlC samples were also bonded to a Ni-based superalloy (Inconel 718) at 1000°C, without evidence of cracking and/or delamination at the interface, but containing a multiphase diffusion zone of approx. 20 μm. [292] On the Cr_2AlC side Ni migrates and Al depletes forming Cr_7C_3, meanwhile the other side is mainly composed of α-Cr(Mo) phase due to outward Ni diffusion. Nevertheless, the system survived 20 thermal cycles from room temperature to 1000°C without cracks, delamination nor surface degradation. Higher temperature and pressure were required to achieve full bonding without cracks or delamination between Ti_2AlC and Inconel 718. The diffusion zone was 60 μm with presence of different zones and compounds, and the system failed after 20 thermal cycles. Interfacial reactions have been also detected between MAX phase coatings (mostly Cr_2AlC) and the metallic substrates. In general the "A" element diffuses into the metal, meanwhile element such as Co, Ti, Mo, Zr or Ni are detected in the MAX phase side.[248,293,294] Diffusion of Al from Cr_2AlC into Zr substrates has been even detected during the annealing treatment at 800°C in vacuum to crystallize the coatings.[295] The diffusion can be suppressed using ZrN and AlN diffusion barriers, which was thermodynamically calculated and experimentally validated for one hour at 1000°C.

5.9 | Precursors of MXenes

MXenes are a new type of 2-Dimensional material that were discovered by Naguib et al in 2011.[22] They are produced by selective chemical etching of the "A" element of MAX phases, followed by a delamination process. In spite of their novelty, MXenes have been attracted massive attention due to the high electrical conductivity, hydrophilicity, huge surface area, and biocompatibility, which lead them to be proposed as cathodes for Li- and Na- batteries, electromagnetic interference shielding, energy storage, water purification and desalination, filtration, sensors, CO catalysts, biosensors, and antibacterial agents.[296,297] Several research groups and industries are interested in MXenes, but so far MAX phase powders are the only precursors. The current huge explosion and demand of these materials might trigger the industrial production of MAX phase powders.

6 | FUTURE CHALLENGES

To accelerate the transfer of MAX phases to the market, research at multiple fronts is required. In that sense, some suggestions are outline to identify and guide high impact investigations.

6.1 | MAX phases and solid solutions

Multiple phases and their structural characterization have been explored, therefore no major issues are left to be addressed in this field. However, investigating new solid solutions and/or doping with catalyst elements such as Pd, Pt, Ni, Mo, Ru, etc would be of interest. In fact, the huge demand and interest in MXenes during the last years have relaunched the synthesis of new phases, such as containing double A-layer (ie Mo_2Ga_2C) and compositions with noble metals as "A" element (ie Ti_2AuN).[298,299] These MAX phases with novel layer-structure/element might exhibit new properties or applications, such as superconductivity or unusual magnetic response. Another aspect is the development of phase diagrams for systems that are difficult to synthesize such as Zr-Al-C.

6.2 | Properties

Most of the work in the last two decades has been focused on the characterization of properties. In general,

mechanisms are well understood, although some open questions remain, ie, the existence of ripplocations, Weibull Modulus, and/or creep mechanisms. The next challenge is to investigate the response under realistic environmental conditions and long exposures (> months). This is particularly determinant for structural materials and coatings for high temperature such as CSP systems and nuclear cladding, but tests require complex infrastructure and are expensive. However, individual parameters (ie water vapor, corrosive particles, CMAS, foreign object impacts, or long exposure) can be readily measured. As mentioned before, catalytic activities have not been explored sufficiently relative to the high potential, number of phases, and vast number of solid solutions/doping. This is an enormous field with many possibilities for future studies.

6.3 | Interfacial reactions

MAX phases have excellent chemical stability with oxide and non-oxide ceramics such as YSZ, Al_2O_3, and SiC. Interactions with superalloys seem to be problematic as some reactions have been detected at interfaces. Unfortunately, the number of experiments, systems and conditions are low. More systems and conditions should be tested to unveiling mechanisms and diffusion rates, but most importantly, different strategies such as the diffusion barriers should be investigated.

6.4 | Synthesis

The main limiting factor to transfer MAX phases to the market is the development of a suitable synthesis process to produce large quantities of highly pure MAX phase powders at affordable costs. If this problem is overcome and high-purity commercial powders are readily available, then components based on MAX phases can be produced for market. Synthesis of MAX powders by SHS method was shown to successfully produce industrial quantities at reasonable prices. However, the purity is not sufficient, particularly if the components must operate at elevated temperatures and in oxidizing environments. Some international companies are seeking large amounts of powders (in the order of tons) but the lack of reliable producers is hindering progress. More efforts and attention are required to synthesize and scale-up MAX phase powders. In that sense, molten salt processes might be an excellent alternative, as they can be used to produce kilograms of powders per batch. Furthermore, novel strategies and different precursors (ie intermetallics, or oxides to reduce costs) have started to be investigated.

6.5 | Structures

Thin films have been largely investigated and they present a huge potential in several applications. More difficulties and clearly less investigations have been performed to obtain thick, dense and highly pure coatings by spray technologies. Investigations should focus on the optimization of MAX powders (ie size, morphology, flowability) and deposition parameters such as gas temperature, particle velocity, spray distance, gas flows, etc Once again, lack of commercial powders has limited the number of groups working on that topic. Similar problems occur for processing of complex shapes, where research groups and industries demand commercial powders with specific characteristics to further investigate.

ACKNOWLEDGMENTS

This work has been funded by the Germany´s Federal Ministry of Education and Research ("Bundesministerium für Bildung und Forschung") under the MAXCOM project (03SF0534). The author gratefully thanks the contributions of his current team and former members to develop some of the experiments and concepts described, in particular to Ms Teresa Go, Mr Sylvain Badie, Mr Rimy Gabriel, Ms Melina Poll, Mr Apurv Dash, Ms Sara Onrubia, and Mr Soheil Karimi. The author would like also to acknowledge Dr Clio Azina for her corrections and comments, Prof. Olivier Guillon, Prof. Robert Vassen, Dr Martin Bram, and Dr Jürgen Malzbender for their valuable discussions and Dr Doris Sebold, Dr Yoo Jung Sohn, Mr Ralf Steinert, Volker Bader, and Mr Frank Kurze for their support in the characterization and experimental work. Open access funding enabled and organized by Projekt DEAL.

ORCID

Jesus Gonzalez-Julian https://orcid.org/0000-0002-4217-8419

REFERENCES

1. Jeitschko W. Kohlenstoffhaltige ternäre Verbindungen (H-Phase). Mh Chem. 1963;332:2–6.
2. Jeitschko W, Nowotny H, Benesovsky F. Ti_2AlN, eine stickstoffhaltige H-Phase. Monatshefte für Chemie. 1963;94(6):1198–200.
3. Jeitschko W. Die kristallstruktur von Ti_3SiC_2- ein neuer komplex-carbid-typ. Mh Chem. 1966;171(1965).
4. Nickl JJ, Schweitzer KK, Luxenberg P. Gasphasenabscheidung im Systeme Ti-C-Si. J Less-Common Met. 1972;26:335–53.
5. Barsoum MW, El-raghy T. Synthesis and characterization of a remarkable ceramic Ti_3SiC_2. J Am Ceram Soc. 1996;79(7):1953–6.
6. Barsoum MW. The MN+1AXN Phases: A New Class of Solids: Thermodynamically Stable Nanolaminates. Prog Solid State Chem. 2000;28(1–4):201–81.
7. Radovic BM, Barsoum MW. MAX phases : Bridging the gap between metals and ceramics. Am Ceram Soc Bull. 2013;92(3):20–7.
8. Sokol M, Natu V, Kota S, Barsoum MW. On the chemical diversity of the MAX phases. Cell Press Rev. 2019;1(2):210–23.

9. Meng FL, Zhou YC, Wang JY. Strengthening of Ti_2AlC by substituting Ti with V. Scr Mater. 2005;53(12):1369–72.
10. Zhang HB, Zhou YC, Bao YW, Li MS. Improving the oxidation resistance of Ti_3SiC_2 by forming a $Ti_3Si_{0.9}Al_{0.1}C_2$ solid solution. Acta Mater. 2004;52(12):3631–7.
11. Gao H, Benitez R, Son W, Arroyave R, Radovic M. Structural, physical and mechanical properties of $Ti_3(Al_{1-x}Si_x)C_2$ solid solution with x=0–1. Mater Sci Eng A. 2016;676:197–208.
12. Du YL, Sun ZM, Hashimoto H, Barsoum MW. Theoretical investigations on the elastic and thermodynamic properties of $Ti_2AlC_{0.5}N_{0.5}$ solid solution. Phys Lett A. 2009;374(1):78–82.
13. Yu W, Mauchamp V, Cabioc'H T, Magne D, Gence L, Piraux L, et al. Solid solution effects in the $Ti_2Al(CxNy)$ MAX phases: Synthesis, microstructure, electronic structure and transport properties. Acta Mater. 2014;80:421–34.
14. Naguib M, Bentzel GW, Shah J, Halim J, Caspi EN, Lu J, et al. New Solid solution MAX phases: $(Ti_{0.5}, V_{0.5})_3AlC_2$, $(Nb_{0.5}, V_{0.5})_2AlC$, $(Nb_{0.5}, V_{0.5})_4AlC_3$ and $(Nb_{0.8}, Zr_{0.2})_2AlC$. Mater Res Lett. 2014;2(4):233–40.
15. Liu Z, Zheng L, Sun L, Qian Y, Wang J, Li M. $(Cr_{2/3}Ti_{1/3})_3AlC_2$ and $(Cr_{5/8}Ti_{3/8})_4AlC_3$: New MAX-phase compounds in Ti-Cr-Al-C system. J Am Ceram Soc. 2014;97(1):67–9.
16. Liu Z, Wu E, Wang J, Qian Y, Xiang H, Li X, et al. Crystal structure and formation mechanism of $(Cr_{2/3}Ti_{1/3})_3AlC_2$ MAX phase. Acta Mater. 2014;73:186–93.
17. Caspi EN, Chartier P, Porcher F, Damay F, Cabioc'h T. Ordering of (Cr, V) layers in nanolamellar $(Cr_{0.5}V_{0.5})N+1ALCN$ compounds. Mater Res Lett. 2015;3(2):100–6.
18. Anasori B, Halim J, Lu J, Voigt CA, Hultman L, Barsoum MW. Mo_2TiAlC_2: A new ordered layered ternary carbide. Scr Mater. 2015;101:5–7.
19. Azina C, Tunca B, Petruhins A, Xin B, Yildizhan M, Persson POA, et al. Deposition of MAX phase containing thin films from a $(Ti,Zr)_2AlC$ compound target. arXiv:190904097. 2020.
20. Barsoum MW. MAX Phases: Properties of Machinable Ternary Carbides and Nitrides. Wiley VCH. 2013.
21. National Science and Technology Council. Materials Genome Initiative for Global Competitiveness. 2011.
22. Naguib M, Kurtoglu M, Presser V, Lu J, Niu J, Heon M, et al. Two-dimensional nanocrystals produced by exfoliation of Ti_3AlC_2. Adv Mater. 2011;23(37):4248–53.
23. Sun ZM. Progress in research and development on MAX phases: a family of layered ternary compounds. Int Mater Rev. 2011;56(3):143–66.
24. Barsoum MW, Radovic M. Elastic and mechanical properties of the MAX phases. Annu Rev Mater Res. 2011;41(1):195–227.
25. Tallman DJ, Anasori B, Barsoum MW. A critical review of the oxidation of Ti_2AlC, Ti_3AlC_2 and Cr_2AlC in Air. Mater Res Lett. 2013;1(3):115–25.
26. Gupta S, Barsoum MW. On the tribology of the MAX phases and their composites during dry sliding: a review. Wear. 2011;271(9–10):1878–94.
27. Ingason AS, Dahlqvist M, Rosen J. Magnetic MAX phases from theory and experiments: a review. J Phys Condens Matter. 2016;28(43).
28. Kushima A, Qian X, Zhao P, Zhang S, Li J. Ripplocations in van der Waals layers. Nano Lett. 2015;15(2):1302–8.
29. Gruber J, Lang AC, Griggs J, Taheri ML, Tucker GJ, Barsoum MW. Evidence for bulk ripplocations in layered solids. Sci Rep. 2016;6:1–8.
30. Griggs J, Lang AC, Gruber J, Tucker GJ, Taheri ML, Barsoum MW. Spherical nanoindentation, modeling and transmission electron microscopy evidence for ripplocations in Ti_3SiC_2. Acta Mater. 2017;131:141–55.
31. Barsoum MW, Zhao X, Shanazarov S, Romanchuk A, Koumlis S, Pagano SJ, et al. Ripplocations: A universal deformation mechanism in layered solids. Phys Rev Mater. 2019;3(1):1–9.
32. Barsoum MW, Zhen T, Kalidindi SR, Radovic M, Murugaiah A. Fully reversible, dislocation-based compressive deformation of Ti_3SiC_2 to 1 GPa. Nat Mater. 2003;2(2):107–11.
33. Gilbert CJ, Bloyer DR, Barsoum MW, Tomsia AP, Ritchie RO.Fatigue-crack growth and fracture properties of coarse and fine-grained Ti3SiC2. 2000;42:761–7.
34. Hu C, Sakka Y, Grasso S, Nishimura T, Guo S, Tanaka H. Shell-like nanolayered Nb_4AlC_3 ceramic with high strength and toughness. Scr Mater. 2011;64(8):765–8.
35. Radovic M, Barsoum MW, Seidensticker J, Wiederhorn S. Tensile properties of Ti_3SiC_2 in the 25 ± 1300°C temperature range. 2000;48:453–9.
36. El-Raghy T, Wiederhorn S, Luecke W, Radovic M, Barsoum M. Effect of temperature, strain rate and grain size on the mechanical response of Ti_3SiC_2 in tension. Acta Mater. 2002;50(6):1297–306.
37. Radovic M, Barsoum MW, El-Raghy T, Wiederhorn SM. Tensile creep of coarse-grained Ti_3SiC_2 in the 1000–1200°C temperature range. J Alloys Compd. 2003;361(1–2):299–312.
38. Tallman DJ, Naguib M, Anasori B, Barsoum MW. Tensile creep of Ti_2AlC in air in the temperature range 1000–1150°C. Scr Mater. 2012;66(10):805–8.
39. Zhang H, Wang X, Wan P, Zhan X, Zhou Y. Insights into high temperature uniaxial compression deformation behavior of Ti_3AlC_2. J Am Ceram Soc. 2015;98(10):3332–7.
40. Radovic M, Barsoum MW, Wiederhorn S. Tensile creep of fine grained (3–5 μm) Ti_3SiC_2 in the 1000–1200°C temperature range. Acta Mater. 2001;49:4103–12.
41. Drouelle E, Joulain A, Cormier J, Gauthier-Brunet V, Villechaise P, Dubois S, et al. Deformation mechanisms during high temperature tensile creep of Ti_3AlC_2 MAX phase. J Alloys Compd. 2017;693:622–30.
42. Araki W, Gonzalez-Julian J, Malzbender J. High temperature compressive creep of dense and porous Cr_2AlC in air. J Eur Ceram Soc. 2019;39(13):3660–7.
43. Li X, Gonzalez-Julian J, Malzbender J. Fabrication and mechanical performance of Ti_2AlN prepared by FAST/SPS. J Eur Ceram Soc. 2020;40:4445–53.
44. Li S, Li H, Zhou Y, Zhai H. Mechanism for abnormal thermal shock behavior of Cr_2AlC. J Eur Ceram Soc. 2014;34(5):1083–8.
45. Li H, Li S, Zhou Y. Cyclic thermal shock behaviour of a Cr_2AlC ceramic. Mater Sci Eng A. 2014;607:525–9.
46. Zhang HB, Zhou YC, Bao YW, Li MS.Abnormal thermal shock behavior of Ti_3SiC_2 and Ti_3AlC_2. 2006;21(9):2401–7.
47. El-raghy T, Barsoum MW, Zavaliangos A, Kalidindi SR. Processing and mechanical properties of Ti_3SiC_2: II, Effect of Grain Size and deformation temperature. J Am Ceram Soc. 1999;82(10):2855–60.
48. Bao YW, Wang XH, Zhang HB, Zhou YC. Thermal shock behavior of Ti_3AlC_2 from between 200°C and 1300°C. J Eur Ceram Soc. 2005;25(14):3367–74.
49. Procopio AT, Barsoum MW, El-raghy T. Characterization of Ti_4AlN_3. Metall Mater Trans A. 2000;31:333–7.
50. Hu C, He L, Liu M, Wang X, Wang J, Li M, et al. In situ reaction synthesis and mechanical properties of V_2AlC. J Am Ceram Soc. 2008;91(12):4029–35.

51. Ganguly A, Zhen T, Barsoum MW. Synthesis and mechanical properties of Ti_3GeC_2 and $Ti_3(Si_xGe_{1-x})C_2$ (x = 0.5, 0.75) solid solutions. J Alloys Compd. 2004;376(1–2):287–95.
52. Bao YW, Zhou YC, Zhang HB. Investigation on reliability of nanolayer-grained Ti_3SiC_2 via Weibull statistics. J Mater Sci. 2007;42(12):4470–5.
53. Smialek JL. Oxidation of Al_2O_3 Scale-Forming MAX Phases in Turbine Environments. Metall Mater Trans A Phys Metall Mater Sci. 2017;1–11.
54. Gupta S, Barsoum MW. Synthesis and oxidation of V_2AlC and $(Ti_{0.5}, V_{0.5})_2AlC$ in air. J Electrochem Soc. 2004;151(2):24–9.
55. Azina C, Mráz S, Hans M, Primetzhofer D, Schneider JM, Eklund P. Oxidation behaviour of V_2AlC MAX phase coatings. J Eur Ceram Soc. 2020;40(13):4436–44.
56. Gupta S, Filimonov D, Barsoum MW. Isothermal oxidation of Ta_2AlC in air. J Am Ceram Soc. 2006;89(9):2974–6.
57. Salama I, El-Raghy T, Barsoum MW. Oxidation of Nb_2AlC and $(Ti, Nb)_2AlC$ in air. J Electrochem Soc. 2003;150(3):152–8.
58. Smialek JL. Oxygen diffusivity in alumina scales grown on Al-MAX phases. Corros Sci. 2015;91:281–6.
59. Yu W, Vallet M, Levraut B, Gauthier-Brunet V, Dubois S. Oxidation mechanisms in bulk Ti_2AlC: influence of the grain size. J Eur Ceram Soc. 2020;40(5):1820–8.
60. Shang L, Pradeep KG, Sandlöbes S, to Baben M, Schneider JM. Effect of Si additions on the Al_2O_3 grain refinement upon oxidation of Cr_2AlC MAX phase. J Eur Ceram Soc. 2017;37(4):1339–47.
61. Xu L, Zhu D, Liu Y, Suzuki TS, Kim B, Sakka Y, et al. Effect of texture on oxidation resistance of Ti_3AlC_2. J Eur Ceram Soc. 2018;38(10):3417–23.
62. Smialek JL. Unusual Oxidative Limitations for Al-MAX Phases. 2017;NASA/TM-219444.
63. Yang HJ, Pei YT, Rao JC, De Hosson JTM, Li SB, Song GM. High temperature healing of Ti_2AlC: On the origin of inhomogeneous oxide scale. Scr Mater. 2011;65(2):135–8.
64. Sundberg M, Malmqvist G, Magnussion A, El-Raghy T. Alumina forming high temperature silicides and carbides. Ceram Int. 2004;30:1899–904.
65. Cui B, Jayaseelan DD, Lee WE. Microstructural evolution during high-temperature oxidation of Ti_2AlC ceramics. Acta Mater. 2011;59(10):4116–25.
66. Gibson JSKL, Gonzalez-Julian J, Krishnan S, Vaßen R, Korte-Kerzel S. Mechanical characterisation of the protective Al_2O_3 scale in Cr_2AlC MAX phases. J Eur Ceram Soc. 2019;39(16):5149–55.
67. Lee DB, Nguyen TD, Han JH, Park SW. Oxidation of Cr_2AlC at 1300°C in air. Corros Sci. 2007;49(10):3926–34.
68. Smialek JL, Nesbitt JA, Gabb TP, Garg A, Miller RA. Hot corrosion and low cycle fatigue of a Cr_2AlC-coated superalloy. Mater Sci Eng A. 2018;711:119–29.
69. Smialek JL, Gray S. Type II hot corrosion screening tests of a Cr_2AlC MAX phase compound. Oxid Met. 2018;90(5):555–70.
70. Basu S, Obando N, Gowdy A, Karaman I, Radovic M. Long-term oxidation of Ti_2AlC in air and water vapor at 1000–1300°C temperature range. J Electrochem Soc. 2012;159(2):90–6.
71. Smialek JL. Environmental resistance of a Ti_2AlC-type MAX phase in a high pressure burner rig. J Eur Ceram Soc. 2017;37(1):23–34.
72. Gonzalez-Julian J, Go T, Mack DE, Vaßen R. Environmental resistance of Cr_2AlC MAX phase under thermal gradient loading using a burner rig. J Am Ceram Soc. 2018;101:1841–6.
73. Smialek JL, Cuy MD, Harder BJ, Garg A, Rogers RB. Durability of YSZ coated Ti_2AlC in 1300°C high velocity burner rig tests. J Am Ceram Soc. 2020;in press.
74. Song GM, Pei YT, Sloof WG, Li SB, De Hosson JTM, van der Zwaag S. Oxidation-induced crack healing in Ti_3AlC_2 ceramics. Scr Mater. 2008;58(1):13–6.
75. Li S, Song G, Kwakernaak K, van der Zwaag S, Sloof WG. Multiple crack healing of a Ti_2AlC ceramic. J Eur Ceram Soc. 2012;32(8):1813–20.
76. Li S, Xiao L, Song G, Wu X, Sloof WG, van der Zwaag S. Oxidation and crack healing behavior of a fine-grained Cr_2AlC ceramic. J Am Ceram Soc. 2013;96(3):892–9.
77. Pei R, McDonald SA, Shen L, van der Zwaag S, Sloof WG, Withers PJ, et al. Crack healing behaviour of Cr_2AlC MAX phase studied by X-ray tomography. J Eur Ceram Soc. 2017;37(2):441–50.
78. Yang HJ, Pei YT, De Hosson JTM. Oxide-scale growth on Cr_2AlC ceramic and its consequence for self-healing. Scr Mater. 2013;69(2):203–6.
79. Farle ASM, Stikkelman J, van der Zwaag S, Sloof WG. Oxidation and self-healing behaviour of spark plasma sintered Ta_2AlC. J Eur Ceram Soc. 2017;37(5):1969–74.
80. Farle AS, Kwakernaak C, van der Zwaag S, Sloof WG. A conceptual study into the potential of Mn+1AXn-phase ceramics for self-healing of crack damage. J Eur Ceram Soc. 2015;35(1):37–45.
81. Sloof WG, Pei R, McDonald SA, Fife JL, Shen L, Boatemaa L, et al. Repeated crack healing in MAX-phase ceramics revealed by 4D in situ synchrotron X-ray tomographic microscopy. Sci Rep. 2016;6:23040.
82. Shen L, Eichner D, Van Der ZS, Leyens C, Sloof WG. Reducing the erosive wear rate of Cr_2AlC MAX phase ceramic by oxidative healing of local impact damage. Wear. 2016;358–359:1–6.
83. Lin Z, Zhou Y, Li M, Wang J. Hot corrosion and protection of Ti_2AlC against Na_2SO_4 salt in air. J Eur Ceram Soc. 2006;26(16):3871–9.
84. Wang XH, Zhou YC. Hot corrosion of Na_2SO_4-coated Ti_3AlC_2 in air at 700–1000°C. J Electrochem Soc. 2004;151(9):505–11.
85. Lin ZJ, Li MS, Wang JY, Zhou YC. High-temperature oxidation and hot corrosion of Cr_2AlC. Acta Mater. 2007;55(18):6182–91.
86. Van LK, Lapauw T, Ozalp N, Ström E, Lambrinou K, Vleugels J. Compatibility of SiC-and MAX phase-based ceramics with a KNO_3 -$NaNO_3$ molten solar salt. Sol Energy Mater Sol Cells. 2019;195:228–40.
87. Lapauw T, Tunca B, Joris J, Jianu A, Fetzer R, Weisenburger A, et al. Interaction of Mn+1AXn phases with oxygen-poor, static and fast-flowing liquid lead-bismuth eutetic. J Nucl Mater. 2019;in press.
88. Tunca B, Lapauw T, Callaert C, Hadermann J, Delville R, Caspi E, et al. Compatibility of Zr_2AlC MAX phase-based ceramics with oxygen-poor, static liquid lead-bismuth eutectic. Corros Sci. 2020;171:108704.
89. Guo L, Yan Z, Wang X, He Q. Ti_2AlC MAX phase for resistance against CMAS attack to thermal barrier coatings. Ceram Int. 2019;45:7627–34.
90. Chunfeng H, Fangzhi L, Lingfeng H, Mingyue L, Jie Z, Jiemin W, et al. In situ reaction synthesis, electrical and thermal, and mechanical properties of Nb_4AlC_3. J Am Ceram Soc. 2008;91(7):2258–63.
91. Hu C, Sakka Y, Tanaka H, Nishimura T, Grasso S. Low temperature thermal expansion, high temperature electrical conductivity, and mechanical properties of Nb_4AlC_3 ceramic

synthesized by spark plasma sintering. J Alloys Compd. 2009;487(1–2):675–81.
92. Cabioch T, Eklund P, Mauchamp V, Jaouen M, Barsoum MW. Tailoring of the thermal expansion of $Cr_2(Al_x, Ge_{1-x})C$ phases. J Eur Ceram Soc. 2013;33(4):897–904.
93. Scabarozi TH, Amini S, Leaffer O, Ganguly A, Gupta S, Tambussi W, et al. Thermal expansion of select Mn+1AXn(M=early transition metal, A=A group element, X=C or N) phases measured by high temperature x-ray diffraction and dilatometry. J Appl Phys. 2009;105(1):1–8.
94. Smialek JL, Harder BJ, Garg A. Oxidative durability of TBCs on Ti_2AlC MAX phase substrates. Surf Coatings Technol. 2016;285:77–86.
95. Gonzalez-Julian J, Go T, Mack DE, Vaßen R. Thermal cycling testing of TBCs on Cr_2AlC MAX phase substrates. Surf Coatings Technol. 2018;340.
96. Nappé JC, Grosseau P, Audubert F, Guilhot B, Beauvy M, Benabdesselam M, et al. Damages induced by heavy ions in titanium silicon carbide: Effects of nuclear and electronic interactions at room temperature. J Nucl Mater. 2009;385(2):304–7.
97. Liu X, Le Flem M, Béchade JL, Onimus F, Cozzika T, Monnet I. XRD investigation of ion irradiated $Ti_3Si_{0.90}Al_{0.10}C_2$. Nucl Instruments Methods Phys Res Sect B Beam Interact with Mater Atoms. 2010;268(5):506–12.
98. Liu XM, Le Flem M, Béchade JL, Monnet I. Nanoindentation investigation of heavy ion irradiated $Ti_3(Si, Al)C_2$. J Nucl Mater. 2010;401(1–3):149–53.
99. Tallman DJ, Hoffman EN, Caspi EN, Garcia-Diaz BL, Kohse G, Sindelar RL, et al. Effect of neutron irradiation on select MAX phases. Acta Mater. 2015;85:132–43.
100. Clark DW, Zinkle SJ, Patel MK, Parish CM. High temperature ion irradiation effects in MAX phase ceramics. Acta Mater. 2016;105:130–46.
101. Yang T, Wang C, Taylor CA, Huang X, Huang Q, Li F, et al. The structural transitions of Ti_3AlC_2 induced by ion irradiation. Acta Mater. 2014;65:351–9.
102. Wang C, Yang T, Tracy CL, Xiao J, Liu S, Fang Y, et al. Role of the X and n factors in ion-irradiation induced phase transformations of Mn+1AXn phases. Acta Mater. 2018;144:432–46.
103. Huang Q, Han H, Liu R, Lei G, Yan L, Zhou J, et al. Saturation of ion irradiation effects in MAX phase Cr_2AlC. Acta Mater. 2016;110:1–7.
104. Wang C, Yang T, Xiao J, Liu S, Xue J, Huang Q, et al. Structural transitions induced by ion irradiation in V_2AlC and Cr_2AlC. J Am Ceram Soc. 2016;99(5):1769–77.
105. Bowden D, Ward J, Middleburgh S, de Moraes SS, Zapata-Solvas E, Lapauw T, et al. The stability of irradiation-induced defects in Zr_3AlC_2, Nb_4AlC_3 and $(Zr_{0.5}, Ti_{0.5})_3AlC_2$ MAX phase-based ceramics. Acta Mater. 2020;183:24–35.
106. Myhra S, Summers JWB, Kisi EH. Ti_3SiC_2 - a layered ceramic exhibiting ultra-low friction. Matter Lett. 1999;39:6–11.
107. Gupta S. Tribology of MAX phases and their composites. Drexel University. 2006.
108. Gupta S, Filimonov D, Zaitsev V, Palanisamy T, Barsoum MW. Ambient and 550°C tribological behavior of select MAX phases against Ni-based superalloys. Wear. 2008;264:270–8.
109. Gupta S, Filimonov D, Palanisamy T, Barsoum MW. Tribological behavior of select MAX phases against Al_2O_3 at elevated temperatures. Wear. 2008;265(3–4):560–5.
110. Filimonov D, Gupta S, Palanisamy T, Barsoum MW. Effect of applied load and surface roughness on the tribological properties of Ni-based superalloys versus Ta_2AlC/Ag or Cr_2AlC/Ag Composites. Tribol Lett. 2008;33(1):9–20.
111. Huang Z, Zhai H, Guan M, Liu X, Ai M, Zhou Y. Oxide-film-dependent tribological behaviors of Ti_3SiC_2. Wear. 2007;262(9–10):1079–85.
112. El-Raghy T, Blau P, Barsoum MW. Effect of grain size on friction and wear behavior of Ti_3SiC_2. Wear. 2000;238(2):125–30.
113. Qu L, Bei G, Nijemeisland M, Cao D, van der Zwaag S, Sloof WG. Point contact abrasive wear behavior of MAX phase materials. Ceram Int. 2020;46(2):1722–9.
114. Hu C, Zhou Y, Bao Y, Wan D. Tribological properties of polycrystalline Ti_3SiC_2 and Al_2O_3 -reinforced Ti_3SiC_2 composites. J Am Ceram Soc. 2006;89(11):3456–61.
115. Liu Y, Chen J, Zhou Y. Effect of Ti_5Si_3 on wear properties of $Ti_3Si(Al)C_2$. J Eur Ceram Soc. 2009;29(16):3379–85.
116. Gonzalez-Julian J, Llorente J, Bram M, Belmonte M, Guillon O. Novel Cr_2AlC MAX-phase/SiC fiber composites: Synthesis, processing and tribological response. J Eur Ceram Soc. 2017;37:467–75.
117. Gupta S, Filimonov D, Palanisamy T, El-Raghy T, Barsoum MW. Ta_2AlC and Cr_2AlC Ag-based composites—New solid lubricant materials for use over a wide temperature range against Ni-based superalloys and alumina. Wear. 2007;262(11):1479–89.
118. Wan DT, Hu CF, Bao YW, Zhou YC. Effect of SiC particles on the friction and wear behavior of $Ti_3Si(Al)C_2$-based composites. Wear. 2007;262:833–44.
119. Chen H, Du Y, Wang D, Zhang C, Yang G, Liu B, et al. TiC/Ti_3AlC_2–Co plasma-sprayed coatings with excellent high-temperature tribological properties. Ceram Int. 2018;44(18):22520–8.
120. Dey M, Fuka M, Alanazi F, Gupta S. Synthesis and characterization of novel Ni-Ti_3SiC_2 composites. Ceram Eng Sci Proc. 2019;39(3):107–16.
121. Ghosh S, Dunnigan R, Gupta S. Synthesis and tribological behavior of novel wear-resistant PEEK-Ti_3SiC_2 composites. Proc Inst Mech Eng Part J J Eng Tribol. 2017;231(3):422–8.
122. Gupta S, Riyad MF. Synthesis and tribological behavior of novel UHMWPE-Ti_3SiC_2 composites. Polym Compos. 2018;39(1):254–62.
123. Yoo HI, Barsoum MW, El-Raghy T. Ti_3SiC_2 has negligible thermopower. Nature. 2000;407:581–2.
124. Jovic VD, Barsoum MW. Electrolytic cell and electrodes for use in electrochemical processes. US 7.001.494 B2, 2006.
125. Sun Z, Liang Y, Li M, Zhou Y. Preparation of reticulated MAX-phase support with morphology-controllable nanostructured ceria coating for gas exhaust catalyst devices. J Am Ceram Soc. 2010;93(9):2591–7.
126. Belmonte M, Koller M, Moyano JJ, Seiner H, Miranzo P, Osendi MI, et al. Multifunctional 3D-Printed Cellular MAX-Phase Architectures. Adv Mater Technol. 2019;4:1900375.
127. Tian W, Wang P, Zhang G, Kan Y, Li Y, Yan D. Synthesis and thermal and electrical properties of bulk Cr_2AlC. Scr Mater. 2006;54(5):841–6.
128. Dhakal C, Aryal S, Sakidja R, Ching WY. Approximate lattice thermal conductivity of MAX phases at high temperature. J Eur Ceram Soc. 2015;35(12):3203–12.
129. Sun Z, Hashimoto H, Tian W, Zou Y. Synthesis of the MAX phases by pulse discharge sintering. Int J Appl Ceram Technol. 2010;7(6):704–18.
130. Hu CF, Zhou YC, Bao YW. Material removal and surface damage in EDM of Ti_3SiC_2 ceramic. Ceram Int. 2008;34(3):537–41.

131. Hwang SS, Lee SC, Han J, Lee D, Park S. Machinability of Ti_3SiC_2 with layered structure synthesized by hot pressing mixture of TiCx and Si powder. J Eur Ceram Soc. 2012;32(12):3493–500.
132. Eklund P, Beckers M, Jansson U, Högberg H, Hultman L. The Mn+1AXn phases: Materials science and thin-film processing. Thin Solid Films. 2010;518(8):1851–78.
133. Walter C, Sigumonrong DP, El-raghy T, Schneider JM. Towards large area deposition of Cr_2AlC on steel. Thin Solid Films. 2006;515(2):389–93.
134. Wilhelmsson O, Eklund P, Högberg H, Hultman L, Jansson U. Structural, electrical and mechanical characterization of magnetron-sputtered V-Ge–C thin films. Acta Mater. 2008;56(11):2563–9.
135. Shu R, Ge F, Meng F, Li P, Wang J, Huang Q, et al. One-step synthesis of polycrystalline V_2AlC thin films on amorphous substrates by magnetron co-sputtering. Vacuum. 2017;146:106–10.
136. Eklund P, Rosen J, Persson POÅ. Layered ternary Mn+1AXn phases and their 2D derivative MXene: An overview from a thin-film perspective. J Phys D Appl Phys. 2017;50(11):113001–15.
137. Beckers M, Schell N, Martins RMS, Mücklich A, Möller W. Nucleation and growth of Ti_2AlN thin films deposited by reactive magnetron sputtering onto MgO (111). J Appl Phys. 2007;102(7):074916.
138. Li JJ, Qian YH, Niu D, Zhang MM, Liu ZM, Li MS. Phase formation and microstructure evolution of arc ion deposited Cr_2AlC coating after heat treatment. Appl Surf Sci. 2012;263:457–64.
139. Schramm IC, Pauly C, Johansson Jõesaar MP, Eklund P, Schmauch J, Mücklich F, et al. Solid state formation of Ti_4AlN_3 in cathodic arc deposited $(Ti_{1-x}Al_x)Ny$ alloys. Acta Mater. 2017;129:268–77.
140. Hu JJ, Bultman JE, Patton S, Zabinski JS, Ti T. Pulsed laser deposition and properties of Mn+1AXn phase formulated Ti_3SiC_2 thin films. Tribol Lett. 2004;16(1–2):113–22.
141. Lange C, Hopfeld M, Wilke M, Schawohl J, Kups T, Barsoum MW, et al. Pulsed laser deposition from a pre-synthesized Cr 2AlC MAX phase target with and without ion-beam assistance. Phys Status Solidi Appl Mater Sci. 2012;209(3):545–52.
142. Li L, Zhou A, Xu L, Li Z, Wang L. Synthesis of high pure Ti_3AlC_2 and Ti_2AlC powders from TiH_2 powders as Ti source by tube furnace. J Wuhan Univ Technol Mater Sci Ed. 2013;28(5):882–7.
143. Tunca B, Lapauw T, Karakulina OM, Batuk M, Cabioc'h T, Hadermann J, et al. Synthesis of MAX Phases in the Zr-Ti-Al-C System. Inorg Chem. 2017;56(6):3489–98.
144. Chen L, Dahlqvist M, Lapauw T, Tunca B, Wang F, Lu J, et al. Theoretical prediction and synthesis of $(Cr_{2/3}Zr_{1/3})_2AlC$ i-MAX phase. Inorg Chem. 2018;57(11):6237–44.
145. Gonzalez-Julian J, Onrubia S, Bram M, Guillon O. Effect of sintering method on the microstructure of pure Cr_2AlC MAX phase ceramics. J Ceram Soc Japan. 2016;124(4):415–20.
146. Zhang HB, Zhou YC, Bao YW, Li MS, Wang JY. Intermediate phases in synthesis of Ti_3SiC_2 and $Ti_3Si(Al)C_2$ solid solutions from elemental powders. J Eur Ceram Soc. 2006;26(12):2373–80.
147. Gauthier-Brunet V, Cabioc'h T, Chartier P, Jaouen M, Dubois S. Reaction synthesis of layered ternary Ti2AlC ceramic. J Eur Ceram Soc. 2009;29(1):187–94.
148. Tunca B, Lapauw T, Delville R, Neuville DR, Hennet L, Thiaudière D, et al. Synthesis and characterization of double solid solution $(Zr, Ti)_2(Al, Sn)C$ MAX phase ceramics. Inorg Chem. 2019;58(10):6669–83.
149. Li H, Chen D, Zhou J, Zhao JH, He LH. Synthesis of Ti_3SiC_2 by pressureless sintering of the elemental powders in vacuum. Mater Lett. 2004;58(11):1741–4.
150. Panigrahi BB, Chu M-C, Kim Y-I, Cho S-J, Gracio JJ. Reaction synthesis and pressureless sintering of Cr_2AlC powder. J Am Ceram Soc. 2010;1533(26739):1530–3.
151. Ud Din MF, Yang C, Tang Y, Tian Y, Luo Y, Wu Y, et al. Efficient and cost-effective method to synthesize highly purified Ti_4AlN_3 and Ti_2AlN. J Adv Dielectr. 2019;9(1):2–5.
152. Lis J, Pampuch R, Rudnik T, Węgrzyn Z. Reaction sintering phenomena of self-propagating high-temperature synthesis-derived ceramic powders in the Ti-Si-C system. Solid State Ionics. 1997;101–103(PART 1):59–64.
153. Hendaoui A, Andasmas M, Amara A, Benaldjia A, Langlois P, Vrel D. SHS of high-purity MAX compounds in the Ti-Al-C system. Int J Self-Propagating High-Temperature Synth. 2008;17(2):129–35.
154. Yeh CL, Shen YG. Effects of TiC and $A_{l4}C_3$ addition on combustion synthesis of Ti_2AlC. J Alloys Compd. 2009;470(1–2):424–8.
155. Zhou A, Wang C, Ge Z, Wu L. Preparation of Ti_3AlC_2 and Ti_2AlC by self-propagating high-temperature synthesis. J Mater Sci Lett. 2001;20:1971–3.
156. Riley DP, Kisi EH, Wu E, McCallum A. Self-propagating high-temperature synthesis of Ti_3SiC_2 from 3Ti + SiC + C reactants. J Mater Sci Lett. 2003;22(15):1101–4.
157. Łopaciński M, Puszynski J, Lis J. Synthesis of ternary titanium aluminum carbides using self-propagating high-temperature synthesis technique. J Am Ceram Soc. 2001;84(12):3051–3.
158. Bai Y, He X, Wang R, Sun Y, Zhu C, Wang S, et al. High temperature physical and mechanical properties of large-scale Ti_2AlC bulk synthesized by self-propagating high temperature combustion synthesis with pseudo hot isostatic pressing. J Eur Ceram Soc. 2013;33(13–14):2435–45.
159. Kovalev DY, Averichev OA, Luginina MA, Bazhin PM. Phase Formation in the Ti–Al–C System during SHS. Russ J Non-Ferrous Met. 2019;60(1):61–7.
160. Khoptiar Y, Gotman I. Synthesis of dense Ti_3SiC_2-based ceramics by thermal explosion under pressure. J Eur Ceram Soc. 2003;23(1):47–53.
161. Gorshkov VA, Miloserdov PA, Sachkova NV, Luginina MA, Yukhvid VI. SHS Metallurgy of Cr_2AlC MAX Phase-Based Cast Materials. Russ J Non-Ferrous Met. 2018;59(5):570–5.
162. Ho-duc LH, El-raghy T, Barsoum MW. Synthesis and characterization of 0.3 Vf TiC-Ti_3SiC_2 and 0.3 Vf SiC-Ti_3SiC_2 composites. J Alloys Compd. 2003;350:303–12.
163. Guillon O, Gonzalez-Julian J, Dargatz B, Kessel T, Schierning G, Räthel J, et al. Field-assisted sintering technology/spark plasma sintering: mechanisms, materials, and technology developments. Adv Eng Mater. 2014;16(7):830–49.
164. Tian W, Sun Z, Du Y, Hashimoto H. Mechanical properties of pulse discharge sintered Cr_2AlC at 25–1000°C. Mater Lett. 2009;63(8):670–2.
165. Duan X, Shen L, Jia D, Zhou Y, van der Zwaag S, Sloof WG. Synthesis of high-purity, isotropic or textured Cr_2AlC bulk ceramics by spark plasma sintering of pressure-less sintered powders. J Eur Ceram Soc. 2015;35(5):1393–400. Available from: http://linkinghub.elsevier.com/retrieve/pii/S0955221914005949
166. Liu W, Qiu C, Zhou J, Ding Z, Zhou X, Du S, et al. Fabrication of Ti_2AlN ceramics with orientation growth behavior by the microwave sintering method. J Eur Ceram Soc. 2015;35(5):1385–91.
167. Zhou WB, Mei BC, Zhu JQ, Hong XL. Rapid synthesis of Ti_2AlC by spark plasma sintering technique. Mater Lett. 2005;59(1):131–4.

168. Hossein-Zadeh M, Ghasali E, Mirzaee O, Mohammadian-Semnani H, Alizadeh M, Orooji Y, et al. An investigation into the microstructure and mechanical properties of V2AlC MAX phase prepared by microwave sintering. J Alloys Compd. 2019;795:291–303.
169. Guan C. Synthesis of fine and high purity Cr_2AlC powders by novel method. Adv Appl Ceram. 2016;115(8):505–8.
170. Zhou W, Li K, Zhu J, Tian S, Zhu DM. Low-temperature synthesis of high-purity Ti_2AlC powder by microwave sintering. Micro Nano Lett. 2018;13(6):798–800.
171. Chen W, Tang J, Shi X, Ye N, Yue Z, Lin X. Synthesis and formation mechanism of high-purity Ti_3AlC_2 powders by microwave sintering. Int J Appl Ceram Technol. 2020;17(2):778–89.
172. Guan C, Sun N. Synthesis of high-purity Ti_2SC powder by microwave hybrid heating. J Adv Ceram. 2016;5(4):337–43.
173. Wang Q, Hu C, Huang Q, Cai S, Sakka Y, Grasso S. Synthesis of high-purity Ti_3SiC_2 by microwave sintering. Int J Appl Ceram Technol. 2014;11(5):911–8.
174. Li F, Zhang H, Wang Q, Qu D, Zhou T, Kim B, et al. Microwave sintering of $Ti_3Si(Al)C_2$ ceramic. J Am Ceram Soc. 2014;97(9):2731–5.
175. Low IM. Ceramic matrix composites. Microstructure, properties and applications. Woodhead Publishing. 2006.
176. Foratirad H, Baharvandi H, Maraghe MG. Effect of excess silicon content on the formation of nano-layered Ti_3SiC_2 ceramic via infiltration of TiC preforms. J Eur Ceram Soc. 2017;37(2):451–7.
177. Shan D, Yan G, Zhou L, Li C, Li J, Liu G, et al. Synthesis of Ti_3SiC_2 bulks by infiltration method. J Alloys Compd. 2011;509(8):3602–5.
178. Hwang SS, Han J, Lee D, Park SW. Synthesis of Ti_3SiC_2 by infiltration of molten Si. J Alloys Compd. 2011;509(35):L336–L339.
179. Ma Y, Yin X, Fan X, Travitzky N, Greil P. Fabrication of MAX-phase-based ceramics by three-dimensional printing. J Ceram Sci Technol. 2015;6(2):87–94.
180. Li S-B, Bei G-P, Zhai H-X, Zhou Y, Li C-W. Synthesis of Ti_2SnC at low-temperature using mechanically activated sintering process. Mater Sci Eng A. 2007;457(1–2):282–6.
181. Lenz F, Krenkel W. Fabrication of fiber composites with a MAX phase matrix by reactive melt infiltration. IOP Conf Ser Mater Sci Eng. 2011;18(20):202030.
182. Lu CY, Yin XW, Li XM. A novel in-situ synthesis route of Ti_3SiC_2-SiC composite by liquid silicon infiltration. Journal Inorg Mater. 2010;25(9):1003–8.
183. Tian WB, Wang PL, Kan YM, Zhang GJ. Cr_2AlC powders prepared by molten salt method. J Alloys Compd. 2008;461(1–2):6–11.
184. Galvin T, Hyatt NC, Rainforth WM, Reaney IM, Shepherd D. Molten salt synthesis of MAX phases in the Ti-Al-C system. J Eur Ceram Soc. 2018;38(14):4585–9.
185. Guo X, Wang J, Yang S, Gao L, Qian B. Preparation of Ti_3SiC_2 powders by the molten salt method. Mater Lett. 2013;111:211–3.
186. Wang B, Zhou A, Hu Q, Wang L. Synthesis and oxidation resistance of V2AlC powders by molten salt method. Int J Appl Ceram Technol. 2017;14(5):873–9.
187. Yang LX, Wang Y, Zhang HL, Liu HJ, Zeng CL. A simple method for the synthesis of nanosized Ti_3AlC_2 powder in NaCl–KCl molten salt. Mater Res Lett. 2019;7(9):361–7.
188. Dash A, Vaßen R, Guillon O, Gonzalez-julian J. Molten salt shielded synthesis of oxidation prone materials in air. Nat Mater. 2019;18:465–70.
189. Dash A, Gonzalez-Julian J, Vaßen R, Guillon O. Verfahren zur Herstellung von nicht oxidischen, keramischen Pulvern. 102017006658.2, 2017.
190. Dash A, Sohn YJ, Vaßen R, Guillon O, Gonzalez-Julian J. Synthesis of Ti_3SiC_2 MAX phase powder by a molten salt shielded synthesis (MS3) method in air. J Eur Ceram Soc. 2019;39(13):3651–9.
191. Roy C, Banerjee P, Bhattacharyya S. Molten salt shielded synthesis (MS3) of Ti_2AlN and V2AlC MAX phase powders in open air. J Eur Ceram Soc. 2020;40(3):923–9.
192. Abdelkader AM. Molten salts electrochemical synthesis of Cr_2AlC. J Eur Ceram Soc. 2016;36(1):33–42.
193. Li S, Zou X, Xiong X, Zheng K, Lu X, Zhou Z, et al. Electrosynthesis of Ti_3AlC_2 from oxides/carbon precursor in molten calcium chloride. J Alloys Compd. 2018;735:1901–7.
194. Lu J, Luo K. Synthesis of MAX phases Nb_2CuC and $Ti_2(Al_{0.1}Cu_{0.9})N$ by A-site replacement reaction in molten salts. Mater Res Bull. 2019;7(12):510–6.
195. Badie S, Dash A, Sohn YJ, Vassen R, Guillon O, Gonzalez-Julian J. Synthesis, sintering and effect of surface roughness on oxidation of submicron Ti_2AlC. J Am Ceram Soc. 2020;accepted..
196. Hu C, Sakka Y, Tanaka H, Nishimura T, Grasso S. Fabrication of textured Nb_4AlC_3 ceramic by slip casting in a strong magnetic field and spark plasma sintering. J Am Ceram Soc. 2011;94(2):410–5.
197. Hu C, Sakka Y, Grasso S, Suzuki TS, Tanaka H. Tailoring Ti_3SiC_2 ceramic via a strong magnetic field alignment method followed by spark plasma sintering. J Am Ceram Soc. 2011;94(3):742–8.
198. Lapauw T, Vanmeensel K, Lambrinou K, Vleugels J. A new method to texture dense Mn+ 1AXn ceramics by spark plasma deformation. Scr Mater. 2016;111:98–101.
199. Hocquet S, Dupont V, Cambier F, Ludewig F, Vandewalle N. Densification of complex shape ceramics parts by SPS. J Eur Ceram Soc. 2020;40(7):2586–96.
200. Manière C, Nigito E, Durand L, Weibel A, Beynet Y, Estournès C. Spark plasma sintering and complex shapes: The deformed interfaces approach. Powder Technol. 2017;320:340–5.
201. Bram M, Laptev A, Prasad Mishra T, Nur K, Kindelmann M, Ihrig M, et al. Application of electric current assisted sintering techniques for the processing of advanced materials. Adv Eng Mater. 2020;22(6):2000051.
202. Tian W, Sun Z, Hashimoto H, Du Y. Synthesis, microstructure and mechanical properties of Ti_3SiC_2-TiC composites pulse discharge sintered from Ti/Si/TiC powder mixture. Mater Sci Eng A. 2009;526:16–21.
203. Yang J, Pan LM, Gu W, Gu XB, Song K, Qiu T, et al. Oxidation behavior and kinetics of in situ $(TiB_2+TiC)/Ti_3SiC_2$ composites in air. Ceram Int. 2012;38(1):159–68.
204. Zhu J, Jiang H, Wang F, Yang C, Xiao D. Synthesis, microstructure and mechanical properties of Cr_2AlC/Al_2O_3 in situ composites by reactive hot pressing. J Eur Ceram Soc. 2014;34(16):4137–44.
205. Li Z, Zhou A, Li L, Wang L, Hu M, Li S, et al. Synthesis and characterization of novel Ti_3SiC_2–cBN composites. Diam Relat Mater. 2014;43:29–33.
206. Tang C, Li T, Gao J, Kang S, Xiong C, Li H, et al. Microstructure and mechanical behavior of the Cf/Ti_3SiC_2-SiC composites fabricated by compression molding and pressureless sintering. Ceram Int. 2017;43(18):16204–9.
207. Lagos MA, Pellegrini C, Agote I, Azurmendi N, Barcena J, Parco M, et al. Ti_3SiC_2-Cf composites by spark plasma sintering:

Processing, microstructure and thermo-mechanical properties. J Eur Ceram Soc. 2019;39(9):2824–30.
208. Spencer CB, Córdoba JM, Obando NH, Radovic M, Odén M, Hultman L, et al. The Reactivity of Ti_2AlC and Ti_3SiC_2 with SiC Fibers and Powders up to Temperatures of 1550°C. J Am Ceram Soc. 2011;94(6):1737–43.
209. Guo S. Improvement of mechanical properties of SiC(SCS-6) fiber-reinforced Ti3AlC2 matrix composites with Ti barrier layer. J Eur Ceram Soc. 2016;36(6):1349–58.
210. Jeon K. Processing and mechanical properties of Ti2AlC reinforced with alumina fibers. Texas A&M University. 2011.
211. Spencer CB, Cõrdoba JM, Obando N, Sakulich A, Radovic M, Odén M, et al. Phase evaluation in Al_2O_3 fiber-reinforced Ti 2AlC during sintering in the 1300°C-1500°C temperature range. J Am Ceram Soc. 2011;94(10):3327–34.
212. Dash A, Malzbender J, Dash K, Rasinski M, Vassen R, Guillon O, et al. Compressive creep of SiC whisker/Ti_3SiC_2 composites at high temperature in air. J Am Ceram Soc. 2020;103:5952–65.
213. Dash A, Malzbender J, Vassen R, Guillon O, Gonzalez-Julian J. Short SiC fiber/Ti3SiC2 MAX phase composites: Fabrication and creep evaluation. J Am Ceram Soc. 2020;accepted.103: 7072–7081.
214. Zhang Y, Sun Z, Zhou Y. Cu/Ti_3SiC_2 composite: a new electrofriction material. Mater Res Innov. 1999;3(2):80–4.
215. Peng L. Fabrication and properties of Ti3AlC2 particulates reinforced copper composites. Scr Mater. 2007;56(9):729–32.
216. Wang XW, Lin LZ, Ting LG, Jia L, Xian CJ. Effect of Cr_2AlC content on the properties of a Cu-Cr_2AlC composite. Results Phys. 2016;6:789–95.
217. Wang WJ, Gauthier-Brunet V, Bei GP, Laplanche G, Bonneville J, Joulain A, et al. Powder metallurgy processing and compressive properties of Ti_3AlC_2/Al composites. Mater Sci Eng A. 2011;530(15):168–73.
218. Yu W, Wang X, Zhao H, Ding C, Huang Z, Zhai H, et al. Microstructure, mechanical properties and fracture mechanism of Ti_2AlC reinforced AZ91D composites fabricated by stir casting. J Alloys Compd. 2017;702:199–208.
219. Amini S, Barsoum MW. On the effect of texture on the mechanical and damping properties of nanocrystalline Mg-matrix composites reinforced with MAX phases. Mater Sci Eng A. 2010;527(16):3707–18.
220. Hanaor DAH, Hu L, Kan WH, Proust G, Foley M, Karaman I, et al. Compressive performance and crack propagation in Al alloy/Ti_2AlC composites. Mater Sci Eng A. 2016;672:247–56.
221. Hu L, Kothalkar A, Proust G, Karaman I, Radovic M. Fabrication and characterization of NiTi/Ti_3SiC_2 and NiTi/Ti_2AlC composites. J Alloys Compd. 2014;610:635–44.
222. Studart AR, Gonzenbach UT, Tervoort E, Gauckler LJ. Processing routes to macroporous ceramics: A review. J Am Ceram Soc. 2006;89(6):1771–89.
223. Liu X, Jiang Y, Zhang H, Yu L, Kang J, He Y. Porous Ti_3SiC_2 fabricated by mixed elemental powders reactive synthesis. J Eur Ceram Soc. 2015;35(4):1349–53.
224. Sun Z, Murugaiah A, Zhen T, Zhou A, Barsoum M. Microstructure and mechanical properties of porous Ti_3SiC_2. Acta Mater. 2005;53(16):4359–66.
225. Velasco B, Ferrari SATB, Gordo E. MAX phases foams produced via a powder metallurgy process using a water soluble spaceholder. Powder Metall. 2014;58(2):95–9.
226. Velasco B, Gordo E, Tsipas SA. MAX phase Ti_2AlC foams using a leachable space-holder material. J Alloys Compd. 2015;646:1036–42.
227. Velasco B, Gordo E, Hu L, Radovic M, Tsipas SA. Influence of porosity on elastic properties of Ti_2AlC and Ti_3SiC_2MAX phase foams. J Alloys Compd. 2018;764:24–35.
228. Hu L, Benitez R, Basu S, Karaman I, Radovic M. Processing and characterization of porous Ti_2AlC with controlled porosity and pore size. Acta Mater. 2012;60(18):6266–77.
229. Zhou CL, Ngai TWL, Lu L, Li YY. Fabrication and characterization of pure porous Ti_3SiC_2 with controlled porosity and pore features. Mater Lett. 2014;131:280–3.
230. Gonzalez-Julian J, Onrubia S, Bram M, Broeckmann C, Vaßen R, Guillon O. High temperature oxidation and compressive strength of Cr_2AlC MAX phase foams with controlled porosity. J Am Ceram Soc. 2018;101:542–52.
231. Araki W, Matsumoto A, Arai Y, Yamada N, Malzbender J, Gonzalez-Julian J. Lifetime estimation of Cr_2AlC MAX phase foam based on long-term oxidation and fracture mechanisms. Materialia. 2020;12:100718.
232. Bowen CR, Thomas T. Macro-porous Ti_2AlC MAX-phase ceramics by the foam replication method. Ceram Int. 2015;41(9):12178–85.
233. Karimi S, Go T, Vassen R, Gonzalez-Julian J. Cr_2AlC MAX phase foams by replica method. Mater Lett. 2019;240:271–4.
234. Potoczek M, Guzi de Moraes E, Colombo P. Ti_2AlC foams produced by gel-casting. J Eur Ceram Soc. 2015;35(9):2445–52.
235. Fey T, Stumpf M, Chmielarz A, Colombo P, Greil P, Potoczek M. Microstructure, thermal conductivity and simulation of elastic modulus of MAX-phase (Ti_2AlC) gel-cast foams. J Eur Ceram Soc. 2018;38(10):3424–32.
236. Elsayed H, Chmielarz A, Potoczek M, Fey T, Colombo P. Direct ink writing of three dimensional Ti_2AlC porous structures. Addit Manuf. 2019;28:365–72.
237. Zhang Z, Lim SH, Chai J, Lai DMY, Cheong AKH, Cheong KL, et al. Plasma spray of Ti_2AlC MAX phase powders: Effects of process parameters on coatings' properties. Surf Coatings Technol. 2017;325:429–36.
238. Pasumarthi V, Chen Y, Bakshi SR, Agarwal A. Reaction synthesis of Ti_3SiC_2 phase in plasma sprayed coating. J Alloys Compd. 2009;484(1–2):113–7.
239. Zhang F, Yan S, Li C, Ding Y, He J, Yin F. Synthesis and characterization of MAX phase Cr_2AlC based composite coatings by plasma spraying and post annealing. J Eur Ceram Soc. 2019;39(16):5132–9.
240. Zhang Z, Lim SH, Chai J, Lai DMY, Lim PC, Cheong AKH, et al. Kerosene-fuelled high velocity oxy-fuel (HVOF) spray of Ti_2AlC MAX phase powders. J Alloys Compd. 2018;735:377–85.
241. Sonestedt M, Frodelius J, Palmquist JP, Högberg H, Hultman L, Stiller K. Microstructure of high velocity oxy-fuel sprayed Ti_2AlC coatings. J Mater Sci. 2010;45(10):2760–9.
242. Frodelius J, Sonestedt M, Björklund S, Palmquist JP, Stiller K, Högberg H, et al. Ti_2AlC coatings deposited by High Velocity Oxy-Fuel spraying. Surf Coatings Technol. 2008;202(24):5976–81.
243. Zhang Z, Lai DMY, Lim SH, Chai J, Wang S, Jin H, et al. Isothermal oxidation of the Ti_2AlC MAX phase coatings deposited by kerosene-fuelled HVOF spray. Corros Sci. 2018;138(1):266–74.
244. Maier BR, Garcia-Diaz BL, Hauch B, Olson LC, Sindelar RL, Sridharan K. Cold spray deposition of Ti_2AlC coatings for improved nuclear fuel cladding. J Nucl Mater. 2015;466:1–6.
245. Gutzmann H, Gärtner F, Höche D, Blawert C, Klassen T. Cold spraying of Ti_2AlC MAX-phase coatings. J Therm Spray Technol. 2013;22(2–3):406–12.

246. Rech S, Surpi A, Vezzù S, Patelli A, Trentin A, Glor J, et al. Cold-spray deposition of Ti_2AlC coatings. Vacuum. 2013;94:69–73.
247. Go T, Sohn YJ, Mauer G, Vaßen R. Cold spray deposition of Cr_2AlC MAX phase for coatings and bond-coat layers. J Eur Ceram Soc. 2019;39(4):860–7.
248. Gonzalez-Julian J, Mauer G, Sebold D, Mack DE, Vassen R. Cr_2AlC MAX phase as bond coat for thermal barrier coatings: Processing, testing under thermal gradient loading, and future challenges. J Am Ceram Soc. 2020;103:2362–75.
249. Yu H, Suo X, Gong Y, Zhu Y, Zhou J, Li H, et al. Ti_3AlC_2 coatings deposited by liquid plasma spraying. Surf Coatings Technol. 2016;299:123–8.
250. Liang Y, Sun Z, Chen J, Liu X, Zhou Y. Electrophoretic deposition of $Ti_3Si(Al)C_2$ from aqueous suspension. J Am Ceram Soc. 2010;93(7):1916–21.
251. Galvin T, Hyatt NC, Rainforth WM, Reaney IM, Shepherd D. Laser sintering of electrophoretically deposited (EPD) Ti_3SiC_2 MAX phase coatings on titanium. Surf Coatings Technol. 2019;366:199–203.
252. Sun Z, Li M, Hu L, Lu X, Zhou Y. Surface chemistry, dispersion behavior, and slip casting of Ti_3AlC_2 suspensions. J Am Ceram Soc. 2009;92(8):1695–702.
253. Gong Y, Tian W, Zhang P, Chen J, Zhang Y, Sun Z. Slip casting and pressureless sintering of Ti_3AlC_2. J Adv Ceram. 2019;8(3):367–76.
254. Galvin T, Hyatt NC, Rainforth WM, Reaney IM, Shepherd D. Slipcasting of MAX phase tubes for nuclear fuel cladding applications. Nucl Mater Energy. 2020;22:100725.
255. Wang L, Aldinger F. Near-net shape forming of advanced ceramics. Adv Eng Mater. 2000;2(3):110–3.
256. Gonzalez-Julian J, Classen L, Bram M, Vassen R, Guillon O. Near net shaping of monolithic and composite MAX phases by injection molding. J Am Ceram Soc. 2016;99(10):3210–3.
257. Stumpf M, Fan X, Biggemann J, Greil P, Fey T. Topological interlocking and damage mechanisms in periodic Ti_2AlC-Al building block composites. J Eur Ceram Soc. 2019;39(6):2003–9.
258. Richardson P, Cuskelly D, Brandt M, Kisi E. Microstructural analysis of in-situ reacted Ti_2AlC MAX phase composite coating by laser cladding. Surf Coatings Technol. 2020;385:125360.
259. Sun W, Dcosta D, Lin F, El-raghy T. Freeform fabrication of Ti_3SiC_2 powder-based structures Part I: Characterization and microstructure evaluation. J Mater Process Technol. 2002;127:343–51.
260. Nan B, Yin X, Zhang L, Cheng L. Three-dimensional printing of Ti_3SiC_2-based ceramics. J Am Ceram Soc. 2011;94(4):969–72.
261. Ma Y, Yin X, Fan X, Wang L, Greil P, Travitzky N. Near-net-shape fabrication of Ti_3SiC_2 -based Ceramics by Three-Dimensional Printing. Int J Appl Ceram Technol. 2015;12(1):71–80.
262. Yin X, Travitzky N, Greil P. Near-net-shape fabrication of Ti_3AlC_2 -based composites. Int J Appl Ceram Technol. 2007;4(2):184–90.
263. Krinitcyn M, Fu Z, Harris J, Kostikov K, Pribytkov GA, Greil P, et al. Laminated Object Manufacturing of in-situ synthesized MAX-phase composites. Ceram Int. 2017;43(12):9241–5.
264. Padture NP, Gell M, Jordan EH. Thermal barrier coatings for gas-turbine engine applications. Science. 2002;296(5566):280–4.
265. Murty KL, Charit I. Structural materials for Gen-IV nuclear reactors: challenges and opportunities. J Nucl Mater. 2008;383:189–95.
266. Alemberti A, Carlsson J, Malambu E, Orden A, Struwe D, Agostini P, et al. European lead fast reactor-ELSY. Nucl Eng Des. 2011;241:3470–80.
267. Bosch J, Bosch RW, Sapundjiev D, Almazouzi A. Liquid metal embrittlement susceptibility of ferriticemartensitic steel in liquid lead alloys. J Nucl Mater. 2008;376:322–9.
268. Fashandi H, Andersson M, Eriksson J, Lu J, Smedfors K, Zetterling CM, et al. Single-step synthesis process of Ti_3SiC_2 ohmic contacts on 4H-SiC by sputter-deposition of Ti. Scr Mater. 2015;99:53–6.
269. Borysiewicz MA, Kamińska E, Piotrowska A, Pasternak I, Jakieła R, Dynowska E. Ti-Al-N MAX phase, a candidate for ohmic contacts to n-GaN. Acta Phys Pol A. 2008;114(5):1061–6.
270. Sommers A, Wang Q, Han X, T'Joen C, Park Y, Jacobi A. Ceramics and ceramic matrix composites for heat exchangers in advanced thermal systems—A review. Appl Therm Eng. 2010;30(11–12):1277–91.
271. Ho CK, Iverson BD. Review of high-temperature central receiver designs for concentrating solar power. Renew Sustain Energy Rev. 2014;29:835–46.
272. Kribus A, Zaibel R, Carey D, Segal A, Karni J. A solar-driven combined cycle power plant. Sol Energy. 1998;62(2):121–9.
273. Licheri R, Musa C, Locci AM, Montinaro S, Orrù R, Cao G, et al. Ultra-high temperature porous graded ceramics for solar energy applications. J Eur Ceram Soc. 2019;39(1):72–8.
274. Fend T, Hoffschmidt B, Pitz-Paal R, Reutter O, Rietbrock P. Porous materials as open volumetric solar receivers: Experimental determination of thermophysical and heat transfer properties. Energy. 2004;29(5–6):823–33.
275. Kearney D, Herrmann U, Nava P, Kelly B, Mahoney R, Pacheco J, et al. Assessment of a molten salt heat transfer fluid in a parabolic trough solar field. J Sol Energy Eng Trans ASME. 2003;125(2):170–6.
276. Mey-Cloutier S, Caliot C, Kribus A, Gray Y, Flamant G. Experimental study of ceramic foams used as high temperature volumetric solar absorber. Sol Energy. 2016;136:226–35.
277. Mastai Y, Polarz S, Antonietti M. Silica-carbon nanocomposites - A new concept for the design of solar absorbers. Adv Funct Mater. 2002;12(3):197–202.
278. Sarwar J, Shrouf T, Srinivasa A, Gao H, Radovic M, Kakosimos K. Characterization of thermal performance, flux transmission performance and optical properties of MAX phase materials under concentrated solar irradiation. Sol Energy Mater Sol Cells. 2018;182:76–91.
279. Carbajo J, Quintanilla A, Garcia-Costa AL, González-Julián J, Belmonte M, Miranzo P, et al. The influence of the catalyst on the CO formation during catalytic wet peroxide oxidation process. Catal Today. 2020;in press.
280. Wang K, Du H, Wang Z, Gao M, Pan H, Liu Y. Novel MAX-phase Ti_3AlC_2 catalyst for improving the reversible hydrogen storage properties of MgH_2. Hydrog Energy. 2017;42(7):4244–51.
281. Ng WHK, Gnanakumar ES, Batyrev E, Sharma SK, Pujari PK, Greer HF, et al. The Ti_3AlC_2 MAX Phase as an Efficient Catalyst for Oxidative Dehydrogenation of n-Butane. Angew Chemie. 2018;130(6):1501–6.
282. Trandafir M, Neatu F, Chirica I, Neatu S, Kuncser A, Cucolea E, et al. Highly efficient ultralow Pd loading supported on MAX phases for chemoselective hydrogenation. ACS Catal. 2020;10(10):5899–908.
283. Yin X, Li M, Xu J, Zhang J, Zhou Y. Direct diffusion bonding of Ti3SiC2 and Ti3AlC2. Mater Res Bull. 2009;44(6):1379–84.
284. Shen L, Xue J, Barsoum MW, Huang Q. Rapid bonding of Ti_3SiC_2 and Ti_3AlC_2 by pulsed electrical current heating. Marshall D, editor. J Am Ceram Soc. 2014;97(12):3721–4.

285. Zhou X, Han YH, Shen X, Du S, Lee J, Huang Q. Fast joining SiC ceramics with Ti_3SiC_2 tape film by electric field-assisted sintering technology. J Nucl Mater. 2015;466:322–7.
286. Fitriani P, Septiadi A, Hyuk JD, Yoon DH. Joining of SiC monoliths using a thin MAX phase tape and the elimination of joining layer by solid-state diffusion. J Eur Ceram Soc. 2018;38(10):3433–40.
287. Tatarko P, Casalegno V, Hu C, Salvo M, Ferraris M, Reece MJ. Joining of CVD-SiC coated and uncoated fibre reinforced ceramic matrix composites with pre-sintered Ti_3SiC_2 MAX phase using Spark Plasma Sintering. J Eur Ceram Soc. 2016;36(16):3957–67.
288. Jiménez C, Mergia K, Lagos M, Yialouris P, Agote I, Liedtke V, et al. Joining of ceramic matrix composites to high temperature ceramics for thermal protection systems. J Eur Ceram Soc. 2016;36(3):443–9.
289. Septiadi A, Fitriani P, Sharma AS, Yoon DH. Low pressure joining of SiCf/SiC composites using Ti_3AlC_2 or Ti_3SiC_2 MAX phase tape. J Korean Ceram Soc. 2017;54(4):340–8.
290. Zhou X, Li Y, Li Y, Liu Z, Yang H, Ding S, et al. Residual thermal stress of SiC/Ti_3SiC_2/SiC joints calculation and relaxed by postannealing. Int J Appl Ceram Technol. 2018;15(5):1157–65.
291. Smialek JL, Garg A. Interfacial reactions of a MAX phase/superalloy hybrid. Surf Interface Anal. 2015;47:844–53.
292. Sokol M, Wang J, Keshavan H, Michel W. Bonding and oxidation protection of Ti_2AlC and Cr_2AlC for a Ni-based Superalloy. J Eur Ceram Soc. 2019;39(4):878–82.
293. Ougier M, Michau A, Lomello F, Schuster F, Maskrot H, Schlegel ML. High-temperature oxidation behavior of HiPIMS as-deposited Cr–Al–C and annealed Cr2AlC coatings on Zr-based alloy. J Nucl Mater. 2020;528:151855.
294. Li J, Jing J, He J, Chen H, Guo H. Microstructure evolution and elemental diffusion behavior near the interface of Cr_2AlC and single crystal superalloy DD5 at elevated temperatures. Mater Des. 2020;193(37):108776.
295. Mráz S, Tyra M, to Baben M, Hans M, Chen X, Herrig F, et al. Thermal stability enhancement of Cr_2AlC coatings on Zr by utilizing a double layer diffusion barrier. J Eur Ceram Soc. 2020;40(4):1119–24.
296. Naguib M, Mochalin VN, Barsoum MW, Gogotsi Y. 25th anniversary article: MXenes: a new family of two-dimensional materials. Adv Mater. 2014;26(7):992–1005.
297. Anasori B, Lukatskaya MR, Gogotsi Y. 2D metal carbides and nitrides (MXenes) for energy storage. Nat Rev Mater. 2017;2(2).
298. Jin S, Su T, Hu Q, Zhou A. Thermal conductivity and electrical transport properties of double-A-layer MAX phase Mo_2Ga_2C. Mater Res Lett. 2020;8(4):158–64.
299. Kashiwaya S, Lai CC, Lu J, Petruhins A, Rosen J, Hultman L. Formation of Ti_2AuN from Au-Covered Ti_2AlN Thin Films: a general strategy to thermally induce intercalation of noble metals into MAX phases. Cryst Growth Des. 2020;20(6):4077–81.

AUTHOR BIOGRAPHY

Jesus Gonzalez-Julian is group leader in the Institute of Energy and Climate Research: Materials Synthesis and Processing (IEK-1) at Forschungszentrum Jülich GmbH (Germany), and Junior Professor in the Institute of Mineral Engineering at RWTH Aachen University. He completed his PhD degree in Inorganic Chemistry at the Institute of Ceramic and Glass and the Universidad Autonoma in Madrid (Spain) developing silicon nitride composites containing carbon nanotubes. Between 2012 and 2014, he went to Germany to undertake post doctoral research at Friedrich-Schiller University Jena, focusing on the understanding of novel sintering techniques such as flash sintering and cold sintering. Furthermore, during this time, he was a guest scientist in the Centre for Advanced Structural Ceramics at Imperial College London (UK) to develop in-situ thermal protection systems in Ultra-High Temperature Ceramics. Then, he moved in 2014 to Forschungszentrum Jülich GmbH to initiate MAX phase activities for high temperature applications, followed by the consolidation of his own group in 2016 thanks to a Young Research Group program of the Germany´s Federal Ministry of Education and Research. His research interests focus on MAX phases and other high temperature ceramics, including synthesis by sustainable processes, processing and near net shaping—from bulk and coatings to foams and additive manufacturing—sintering at low temperature, correlation processing-microstructure-properties, and characterization of properties at high temperature. Despite his youth (36 years old), he has published 70 articles in international peer-reviewed journals, 4 patents, and 6 peer reviewed conference proceedings.

How to cite this article: Gonzalez-Julian J. Processing of MAX phases: From synthesis to applications. *J Am Ceram Soc*. 2021;104:659–690. https://doi.org/10.1111/jace.17544

APPENDIX

Panel A. cold spray deposition of MAX Phases—Potential mechanisms

Cold spraying (CS) is attracting a considerable attention from industries due to the possibility to deposit metallic materials at low temperatures, avoiding the degradation and oxidation of powders and sensitive substrates. In contrast to conventional thermal spray technologies, where the particles are partially or completely molten, CS decreases drastically the temperature at expense of increasing the kinetic energy of the particles. Deposition occurs only at impact velocities higher than a certain material dependent value, which is called critical velocity (Figure P1). At higher velocities, deposition takes place by the deformation of solid particles, and bonding is caused by the strong plastic deformation and shear instability at the interacting surfaces.[1] During impact heat is generated and can facilitate the bonding. However, if the velocity is too high, particles erode the substrate due to their hydrodynamic penetration. Mechanisms are well understood for metallic systems and thick (few millimeters) and dense coatings can be easily achieved. Brittle materials like ceramics cannot be deposit by CS due to the lack of deformation after impact, causing just erosion in the whole range of velocities.

Once more time, MAX phases behave differently due to their unique combination of metallic and ceramic properties, opening the possibility of deposition by CS. The interest of CS resides on the reduction of temperature to avoid the inherent incongruent melting of MAX phases and their potential oxidation. Some successful attempts have been already reported,[2,3,4] although mechanisms are not described and coatings are not fully dense. In that sense, we are currently working on the unveiling of mechanisms and preliminary results show interesting conclusions. Certainly, deposition is caused by the deformation of MAX phase particles under high strain rates (> 10^6 s^{-1}) during the impact, but the main difference with metallic systems is that particle orientation plays a determinant role. The maximal shear deformation of MAX phases occurs at 45° (angle between the basal plane of MAX phases and the substrate surface) due to the layered structure and the weak M-A bonding. At 0° and 90° the plastic deformation is limited, acting more like a ceramic and causing the erosion of the substrate. As particles are randomly distributed during the CS projection, some are deposited (preferential angles of 45°) meanwhile others (at 0° and 90°) would erode the substrate (Figure P1). Deposited particles suffer high deformation, including delamination and formation of kink bands (Figure P1). This suggested mechanism is in good agreement to the orientation of Cr_2AlC coatings reported by CS.[5] Nevertheless, there are still some open questions such as confirmation of this mechanism, efficiency of materials deposition, critical velocity, adhesion particle/substrate, and optimal conditions for deposition including preferential angles as a function of velocity, particle size, gas temperature, etc

Panel B. Breakaway oxidation of Ti_2alc

Among the Al_2O_3 scale-forming MAX phases, Ti_2AlC has attracted a lot of attention due to the excellent oxidation and corrosion resistance up to 1400°C and good CTE match with the oxide scale. The steady-state kinetics have been confirmed as cubic, not parabolic—although sometimes reported, which is consistent with grain-boundary diffusivity of oxygen. Typically, a transient TiO_2 is formed at low temperature (~600°C) and during the first minutes at high temperatures, but these TiO_2-rich nodules generally do not seem to increase. Unfortunately, "generally" cannot be accepted, particularly in aerospace and nuclear applications where MAX phases are targeted, because under some conditions (typically long times) TiO_2 nodules growth massively and uncontrolled (Figure P2). The formation and evolution of these TiO_2 nodules have not been enough investigated, mainly because they are stable, or even consumed, during the first hundreds of hours at temperature between 1100 and 1300°C. Nevertheless, Smialek has already reported the TiO_2 breakaway while spot welding of Ti_2AlC and under other conditions such as long oxidation times (> 3000 h).[6] We are currently investigating the response of MAX phase under realistic operating conditions in terms of environment (high temperature, water vapor,

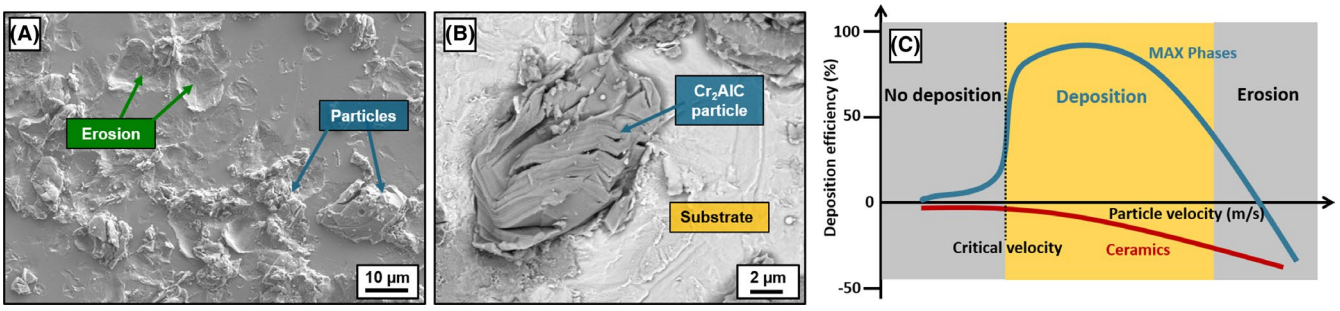

FIGURE P1 A, deposition of Cr_2AlC particles by cold spray, (B) deformation of a Cr_2AlC particle deposited on Inconel 738, (C) graphical representation of the correlation between deposition efficiency and particle velocity for MAX phases and ceramics [Color figure can be viewed at wileyonlinelibrary.com]

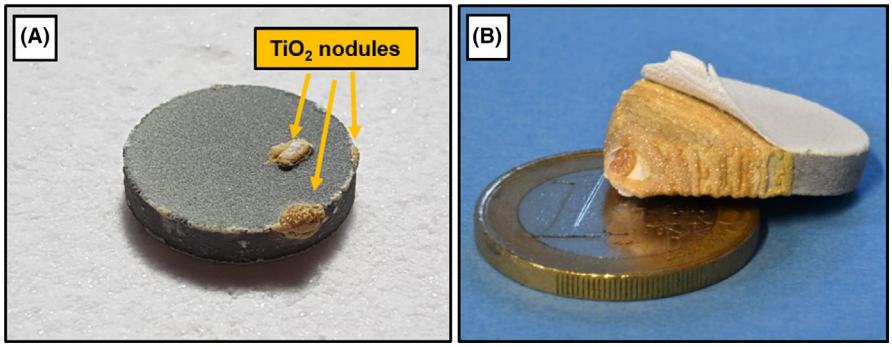

FIGURE P2 A, oxidation of Ti_2AlC at 1200°C under thermal shock conditions and presence of TiO_2nodules, (B) massive and uncontrolled growth of a TiO_2nodule [Color figure can be viewed at wileyonlinelibrary.com]

corrosive particles, etc) and time (> months) in order to determine a potential transfer to industry.

Our preliminary experiments on dense Ti_2AlC samples show the formation of TiO_2 nodules randomly distributed, although with a preferential formation at edges/corners and defects (Figure P2). Most of the nodules are relatively stable and their growth is limited, but in some cases a massive and uncontrolled growth is observed (Figure P2). In that case, the sample might be consumed in a few hundreds of hours. Badie et al[7] are currently investigating this phenomenon in detail and the initial surface roughness seems to play a determinant role. Polished surfaces typically do not present any TiO_2 nodules, while rough (Ra, arithmetical mean roughness > 3 μm), cutting surfaces and sharp angles exhibit them. The reason might be correlated to the stresses generated at these locations between the Ti_2AlC substrate and the alumina scale under thermal shock conditions. After several hours and cycles, the alumina scale might be damage and broken, leading to the continuous and fast formation of TiO_2 due to the oxidation of Ti_2AlC. As Ti_2AlC is not any longer protected by a continuous and adherent alumina layer, the sample can be entirely consumed. Certainly, understanding of formation of these uncontrolled TiO_2 nodules and reasons of the alumina breakdown are mandatory before Ti_2AlC could operate at high temperature in final products.

REFERENCES

1. T. Schmidt, H. Assadi, F. Gärtner, H. Richter, T. Stoltenhoff, H. Kreye, and T. Klassen, "From particle acceleration to impact and bonding in cold spraying," *J Therm. Spray Technol*., **18** [5-6] 794-808 (2009).
2. A. Loganathan, A. Sahu, C. Rudolf, C. Zhang, S. Rengifo, T. Laha, B. Boesl, and A. Agarwal, "Multi-scale tribological and nanomechanical behavior of cold sprayed Ti2AlC MAX phase coating," *Surf. Coatings Technol*., **334** [August 2017] 384-393 (2018).
3. H. Gutzmann, F. Gärtner, D. Höche, C. Blawert, and T. Klassen, "Cold spraying of Ti2AlC MAX-phase coatings," *J Therm. Spray Technol*., **22** [2-3] 406-412 (2013).
4. BR Maier, BL Garcia-Diaz, B. Hauch, LC Olson, RL Sindelar, and K. Sridharan, "Cold spray deposition of Ti2AlC coatings for improved nuclear fuel cladding," *J Nucl. Mater*., **466** 1-6 (2015).
5. T. Go, YJ Sohn, G. Mauer, and R. Vaßen, "Cold spray deposition of Cr2AlC MAX phase for coatings and bond-coat layers," *J Eur. Ceram. Soc*., **39** [4] 860-867 (2019).
6. JL Smialek, *Unusual Oxidative Limitations for Al-MAX Phases*. 2017.
7. S. Badie, A. Dash, YJ Sohn, R. Vassen, O. Guillon, and J. Gonzalez-Julian, "Synthesis, sintering and effect of surface roughness on oxidation of submicron Ti2AlC," *J Am. Ceram. Soc*., submitted (2020).